Precision Engineering 102 (2026) 354–376

Contents lists available at ScienceDirect

Precision Engineering

journal homepage: www.elsevier.com/locate/precision

A novel machining program based on real-time two-variable polynomial calculation for fast tool servo diamond turning of freeform surfaces

Shigeru Tanikawa, Jiwang Yan *

Department of Mechanical Engineering, Faculty of Science and Technology, Keio University, 3-14-1 Hiyoshi, Kohoku-ku, Yokohama, 223-8522, Japan

ARTICLE INFO

Keywords:
Two-variable polynomial fitting
Optical design equation
Freeform surface
Interpolation error
Diamond turning
Fast tool servo

ABSTRACT

Compared with conventional axisymmetric lenses, freeform surfaces provide more flexibility in designing optical lenses and are expected to expand their demand in a wide range of fields, such as virtual and augmented reality and space telescopes. Fast tool servo-based diamond turning is a promising method for machining ultra-precision freeform surfaces. However, interpolation errors occur in machining programs generated with point cloud data, resulting in large form errors, especially for large-size freeform surfaces. To solve this problem, this study proposes a novel machining program that directly evaluates the optical design equation during machining, instead of using conventional point cloud-based machining programs. This method continuously controls the tool position to its ideal position at each control sampling point using two-variable polynomial calculations, thereby reducing interpolation errors. The polynomial coefficients are corrected based on those of the original design equation by considering the tool radius. The freeform surface machining results demonstrate that the proposed method achieves a 75.7% reduction in RMS form error while replacing a point cloud consisting of 993,600 points with only 20 polynomial coefficients. The proposed method also enables machining of multiple surfaces within a single setup, further demonstrating the effectiveness of the proposed machining program. While the form accuracy of the conventional method deteriorates in proportion to the surface curvature and distance from the spindle rotation center, the proposed approach achieves high-precision machining regardless of variations in such factors, distinctly outperforming the conventional bilinear interpolation method.

1. Introduction

The demand for optical elements with freeform surfaces has increased significantly with recent developments in optical lenses [1–3]. Compared to conventional spherical and aspherical lenses, freeform optical elements have high flexibility in optical design and can shorten focal lengths with small aberrations [4–6]. These characteristics also significantly contribute to the design flexibility of products that incorporate optical elements. In addition, although the demand for small lenses, such as smartphone lenses, has been large in recent years, there has also been a growing demand for large-diameter freeform lenses, including lenses for HUDs, VR and AR headsets, and space telescopes [7–9]. To meet these demands, it is necessary to develop machining technologies that can process large freeform optical elements precisely and efficiently.

Conventionally, ultra-precision diamond turning lathes have been used for machining large-diameter freeform optical surfaces [10–12]. There are two types of diamond turning methods: the slow tool servo (STS) and fast tool servo (FTS). STS moves a heavy machine table, resulting in slow back-and-forth motion, although the stroke is long (hundreds of millimeters) [13,14]. In contrast, FTS can achieve fast tool motion by installing a specialized lightweight tool motion unit on a machine table [15,16]. However, the stroke of a conventional piezoelectric-driven FTS is limited to a few micrometers. With the recent development of FTS using voice coil motors, high-speed back-and-forth motion can be precisely controlled over a stroke of a few millimeters using an independent control system. Such newly developed FTS provides new possibilities for the processing of large-diameter freeform surfaces [17–19].

Currently, FTS machining programs use point cloud data to define an ideal surface form [20–22]. By defining the surface using point cloud data, each point can be compensated according to the radius of the round-nosed tool, enabling the machining of precise optical surfaces with minimal form errors [12,23,24]. However, there is a limitation on the number of point clouds that can be read depending on the machining system; for example, up to one million points. For small-diameter

* Corresponding author.
E-mail address: yan@mech.keio.ac.jp (J. Yan).

https://doi.org/10.1016/j.precisioneng.2026.06.019
Received 20 March 2026; Received in revised form 5 June 2026; Accepted 20 June 2026
Available online 22 June 2026

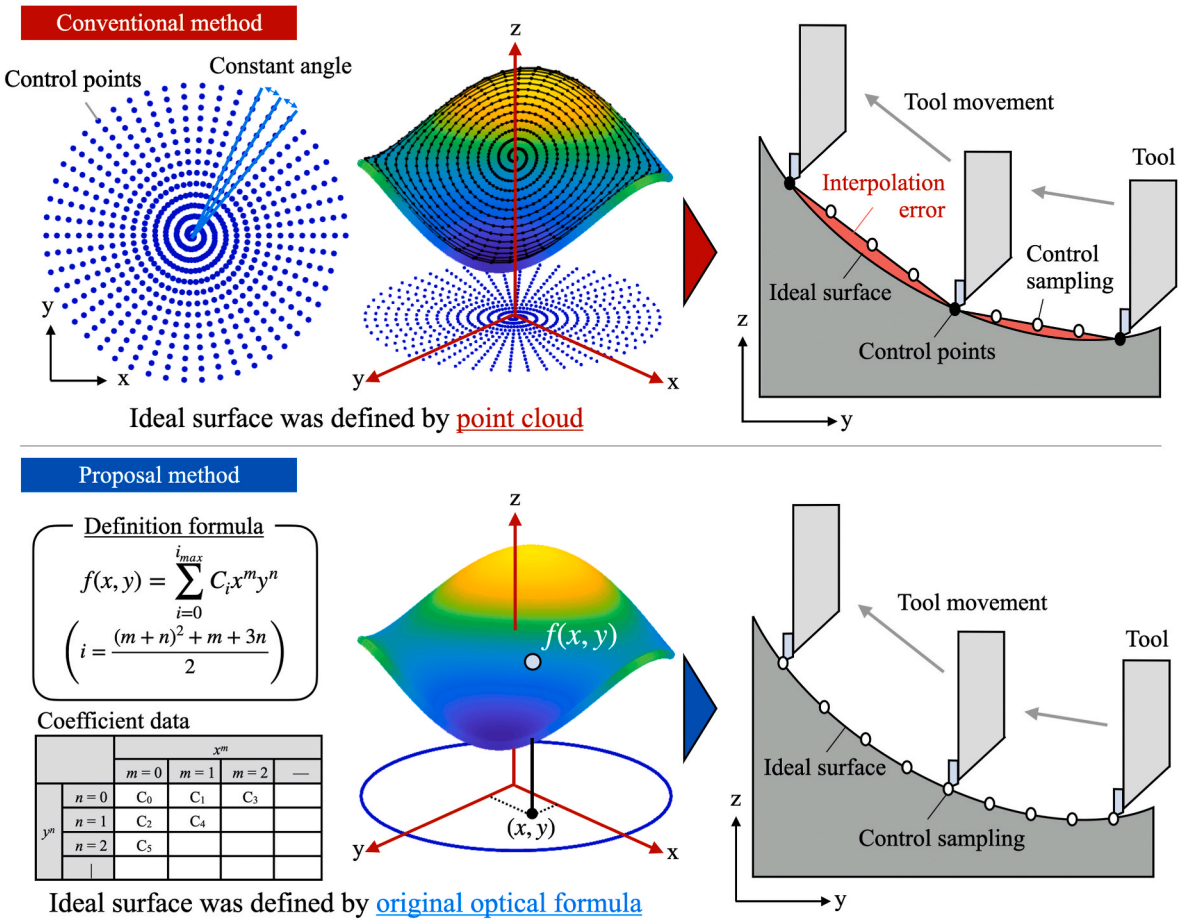

Fig. 1. Overview of the differences in ideal surface definition between the conventional point cloud method and the proposed direct calculation method, and their effects on the machined surface.

freeform surfaces, the error between the polygon surface defined by the point cloud and actual design surface is acceptable. However, as the freeform surface becomes larger, a large interpolation error occurs when attempting to define the form with a limited amount of point cloud data, and this large interpolation error causes an unacceptably large form error in the machined surface. To avoid interpolation errors caused by a limited number of points, many studies have been conducted on the optimization of point cloud arrangements and interpolation methods [25–27]. However, unless the fundamental problem of a limited number of point clouds is eliminated, it is difficult to solve this issue completely.

This study proposes a novel method to solve the problem of point cloud data limitations in independently controlled FTS-based diamond turning. Unlike conventional machining programs written using numerical control (NC) code, in this study, the independently controlled FTS was operated using a program that calculated the corresponding tool position from the input coordinate information of each axis of the base machine based on a two-variable polynomial. To apply tool radius compensation to a machining program, this study proposes a novel compensation method that corrects the coefficients of the design equation according to the tool radius. By utilizing the proposed coefficient correction method, a machining program that calculates the optical design equation in real time during machining was developed to effectively addresses the problem of large volumes of point cloud data required by conventional methods, enabling high-precision and high-efficiency machining of freeform optics.

2. Theory and methods

In optical surface design, a surface is often described using polynomial equations, and its geometry is determined by adjusting the coefficients of the equations. However, when fabricating a designed surface, the geometry is commonly represented as a point cloud. In this study, a novel method for creating a machining program was proposed that calculates the optical design formula during tool movement control based on the loaded coefficients and controls the tool movement according to the calculation results. At each control-sampling step, the design equation was evaluated to compute the target position of the tool. Thus, the tool could be moved in a way that reduces interpolation errors inherent in conventional point cloud methods, enabling higher-precision fabrication. The differences between the conventional point cloud method and the proposed direct calculation method are summarized in Fig. 1. In this section, the fundamental theories and features of optical design, two-variable polynomials, FTS unit control mechanisms, and machining programs are described, and the methodology of the proposed approach is presented.

2.1. Design of optical surface

A conventional aspherical lens shape is defined using the following equation:

$$z(r) = \frac{r^2}{R\left(1+\sqrt{1-\frac{(1+k)r^2}{R^2}}\right)} + \sum_{i=1}^{d} A_{2i} r^{2i}, \tag{1}$$

where z is the height of the designed form, r is the distance from the optical axis, R and k are the curvature radius and conic constant, respectively, d is the maximum coefficient rank, and A_{2i} is the coefficient

Table 1
Correspondence between polynomial exponents and coefficients.

		x^m						
		$m = 0\ (x^0)$	$m = 1\ (x^1)$	$m = 2\ (x^2)$	$m = 3\ (x^3)$	$m = 4\ (x^4)$	$m = 5\ (x^5)$	…
y^n	$n = 0\ (y^0)$	$i = 0\ (C_0)$	$i = 1\ (C_1)$	$i = 3\ (C_3)$	$i = 6\ (C_6)$	$i = 10\ (C_{10})$	$i = 15\ (C_{15})$	
	$n = 1\ (y^1)$	$i = 2\ (C_2)$	$i = 4\ (C_4)$	$i = 7\ (C_7)$	$i = 11\ (C_{11})$	$i = 16\ (C_{16})$		
	$n = 2\ (y^2)$	$i = 5\ (C_5)$	$i = 8\ (C_8)$	$i = 12\ (C_{12})$	$i = 17\ (C_{17})$			
	$n = 3\ (y^3)$	$i = 9\ (C_9)$	$i = 13\ (C_{13})$	$i = 18\ (C_{18})$				
	$n = 4\ (y^4)$	$i = 14\ (C_{14})$	$i = 19\ (C_{19})$					
	$n = 5\ (y^5)$	$i = 20\ (C_{20})$						
	⋮							

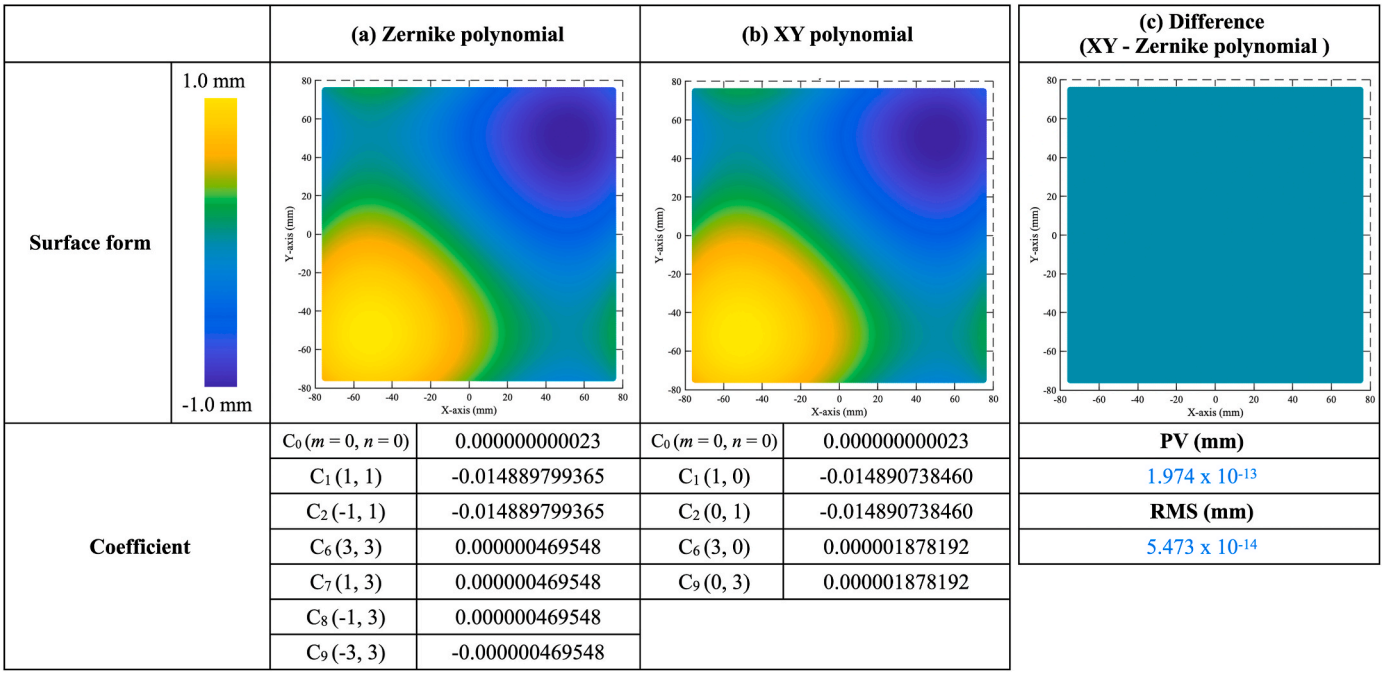

Fig. 2. Freeform surface (a) defined by Zernike polynomial and (b) reproduced by XY polynomial the surface. (c) Difference between the two surfaces shown in (a) and (b).

value [28–30]. The shape of the optical lens is determined by adjusting the value of each coefficient and calculating the ray paths at each wavelength and the optical aberration for the combined state of multiple lenses [31,32]. An equation that explicitly demonstrates the changes in the light path in response to variations in each coefficient is a highly valuable tool in optical design. In particularly, for optical elements that manipulate light and exhibit sensitivity to dimensional changes at the nanometer scale, a formula with numerous finely adjustable coefficients is essential. Thus, although the aspherical surface equation is axially symmetric, it offers a clear interpretation of the role of each coefficient. Owing to its high degree of tunability and precision, the aspherical surface equation has become a widely adopted standard in optical design.

However, the demand for freeform lenses with off-axis target geometries has increased [1–3]. To enable freeform optical design, several polynomial equations have been used to replace conventional aspheric equations. A two-variable polynomial (termed the XY polynomial in this study), in which the distance from the optical axis of the aspheric formula is replaced by x and y coordinates, is now widely used in the design of freeform optical surfaces [11,24,33]. The XY polynomial is expressed as follows:

$$z(x,y) = \sum_{i=0}^{i_{max}} C_i x^m y^n, \tag{2-a}$$

$$i_{max} = \frac{d^2 + 3d + 2}{2} - 1, \tag{2-b}$$

where C_i is the coefficient of the XY polynomial equation, and m and n are exponents of x and y, respectively. This equation is a simple polynomial that compute the sum of all terms by incrementing i from 0 to i_{max}. When the maximum exponents of x and y are the same and the maximum number is d, i_{max} can be calculated using Equation (2-b). The exponents of x and y (m and n) corresponding to index i are listed in Table 1. The XY polynomial has many coefficients, similar to the aspheric equation, and allows for the expression of various freeform surfaces by simply adjusting the coefficient values. The polynomial itself has the property of flexible adjustability by simply changing the coefficients, and this feature is highly compatible with optical lens design. In addition to the XY polynomial, various other polynomials such as the Zernike polynomial have been utilized in optical design formulas [4,34,35]. Although many polynomials are used differently as optical surface definition formulas, depending on the ease of optical design, such as aberration calculations, the final designed surface can be expressed by

		Surface1		Surface2		Combined surface	
Surface form	40 mm / -40 mm	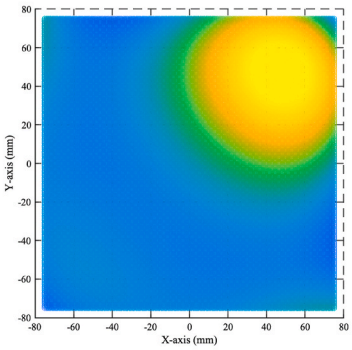		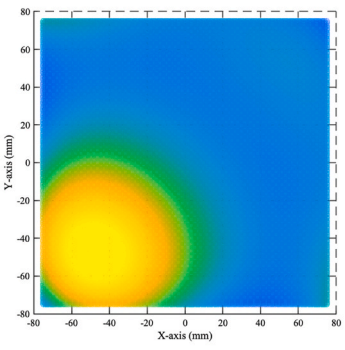		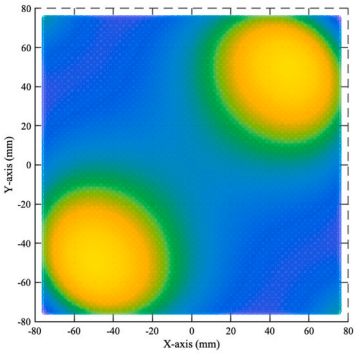	
Coefficient		$C_0\,(m=0, n=0)$	-1.900000000000	$C_0\,(m=0, n=0)$	-1.900000000000	$C_0\,(m=0, n=0)$	-3.800000000000
		$C_1\,(1, 0)$	0.430000000000	$C_1\,(1, 0)$	-0.430000000000	$C_1\,(1, 0)$	0.000000000000
		$C_2\,(0, 1)$	0.430000000000	$C_2\,(0, 1)$	-0.430000000000	$C_2\,(0, 1)$	0.000000000000
		$C_3\,(2, 0)$	0.002200000000	$C_3\,(2, 0)$	0.002200000000	$C_3\,(2, 0)$	0.004400000000
		$C_4\,(1, 1)$	0.012000000000	$C_4\,(1, 1)$	0.012000000000	$C_4\,(1, 1)$	0.024000000000
		$C_5\,(0, 2)$	0.002200000000	$C_5\,(0, 2)$	0.002200000000	$C_5\,(0, 2)$	0.004400000000
		$C_6\,(3, 0)$	-0.000066000000	$C_6\,(3, 0)$	0.000066000000	$C_6\,(3, 0)$	0.000000000000
		$C_7\,(2, 1)$	-0.000004200000	$C_7\,(2, 1)$	0.000004200000	$C_7\,(2, 1)$	0.000000000000
		$C_8\,(1, 2)$	-0.000004200000	$C_8\,(1, 2)$	0.000004200000	$C_8\,(1, 2)$	0.000000000000
		$C_9\,(0, 3)$	-0.000066000000	$C_9\,(0, 3)$	0.000066000000	$C_9\,(0, 3)$	0.000000000000
		$C_{10}\,(4, 0)$	-0.000000510000	$C_{10}\,(4, 0)$	-0.000000510000	$C_{10}\,(4, 0)$	-0.000001020000
		$C_{11}\,(3, 1)$	-0.000001200000	$C_{11}\,(3, 1)$	-0.000001200000	$C_{11}\,(3, 1)$	-0.000002400000
		$C_{12}\,(2, 2)$	0.000000025000	$C_{12}\,(2, 2)$	0.000000025000	$C_{12}\,(2, 2)$	0.000000050000
		$C_{13}\,(1, 3)$	-0.000001200000	$C_{13}\,(1, 3)$	-0.000001200000	$C_{13}\,(1, 3)$	-0.000002400000
		$C_{14}\,(0, 4)$	-0.000000510000	$C_{14}\,(0, 4)$	-0.000000510000	$C_{14}\,(0, 4)$	-0.000001020000

Fig. 3. Example of shape synthesis results obtained by combining the coefficients of different freeform surfaces.

other polynomials often. Fig. 2 shows an example of reproducing a freeform surface represented by certain Zernike coefficients using the XY polynomial coefficients; Fig. 2(a) and (b) compare the freeform surfaces defined by the Zernike and XY polynomials, respectively. The resulting difference, shown in Fig. 2(c), is less than PV 2.0×10^{-13} mm. This indicates that identical surfaces can be obtained, even when defined using different polynomial representations. Therefore, regardless of the polynomial used for designing the optical surface, a machining program developed for one polynomial equation can potentially cover various freeform surfaces defined by other polynomials.

Significant digits		(Original Coef.)	3	6	9	12
Surface form	2.0 mm / -2.0 mm	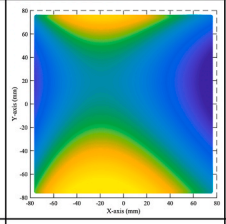	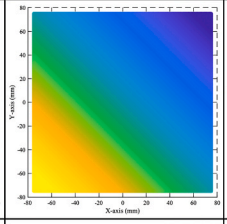	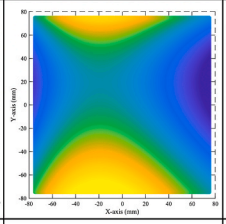	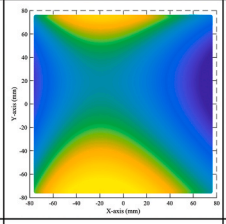	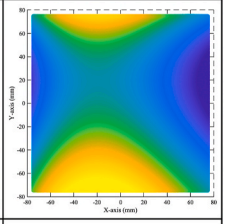
Difference from original	0.001 mm / -0.001 mm	-	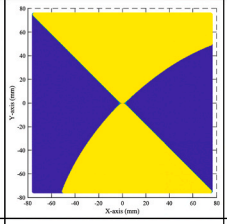	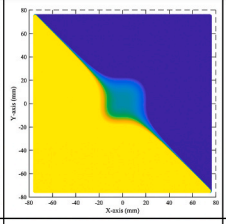	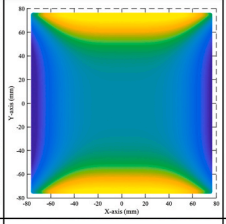	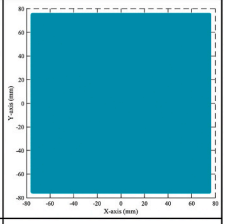
PV (mm)		-	5.3535	0.2055	0.0025	0.0000
RMS (mm)		-	0.9042	0.0276	0.0004	0.0000

Fig. 4. Comparison of freeform surface reproduction accuracy when varying the number of significant digits of the coefficients.

2.2. Features of XY polynomial

In this study, the XY polynomial equation (Equation (2-a)) was treated as the main freeform-defining formula. Despite its simplicity, the XY polynomial can represent various complex freeform optical surfaces and has many other advantages in optical surface machining.

The first advantage is that shapes can be synthesized by simply adding or subtracting coefficients. Fig. 3 shows the results of synthesizing a shape using the coefficients of the XY polynomial. In optical surface machining, this shape composition is useful for creating the corrected ideal surface based on form measurement data [24,34]. When synthesizing shapes from point cloud data, the Z coordinate of one dataset must be recalculated according to the x and y coordinates of the other dataset, and the calculation time depends on the number of point clouds data points and the selected interpolation method. However, the XY polynomial only requires a distinctly smaller amount of data as coefficient values than the point cloud data to synthesize the geometry, and synthesis is achieved by simply adding or subtracting the coefficients.

The second advantage is the ease of scaling the freeform surface. During optical lens fabrication by molding, the shape transferred from the mold to the lens generally shrinks depending on the molding conditions and lens material [33,36,37]. Therefore, pre-expanding the optical surface of the mold is necessary to match the molding shrinkage ratio and obtain a higher-precision lens via molding. Among the many polynomial equations used for optical design, the XY polynomial, which has a simple form, can easily expand or shrink the designed freeform surface as follows:

$$C_i' = \frac{C_i}{s^{(m+n-1)}}, \tag{3}$$

where C_i and C_i' are the coefficients of original and scaled freeform surfaces, respectively, and s is the scaling ratio. If the scaling ratio is greater than 1, the designed freeform surface is enlarged based on this ratio. The values of m and n for specific i are listed in Table 1.

Although the XY polynomial has many attractive features for processing optical freeform surfaces, as described above, careful attention must be paid to the number of significant digits in the coefficients of the equations. Fig. 4 shows the calculated freeform surfaces obtained when varying the number of significant digits of the coefficients and the deviation from the original freeform surface defined by the full-precision coefficients. The comparison results show that the form error of the ideally designed surface has a PV error of a few micrometers when the number of significant digits is set to 12. Based on these results, reading the coefficients to 12 or more decimal places is recommended. When large exponents are used, the number of significant digits in this coefficient must be handled with particular caution.

Freeform surfaces cannot be represented by the XY polynomial equation, such as microlens arrays and high-frequency geometries, which refer to fine, rapidly varying surface features with short spatial wavelengths. Nevertheless, the XY polynomial has many useful properties, as the ability to substitute for other optical design polynomials, such as the Zernike polynomial. Because freeform optical design is often performed using polynomial equations that can be adjusted by changing the coefficients, a machining program specialized for calculating XY polynomials can be broadly applicable to the machining of freeform lens surfaces defined by various optical polynomial equations.

2.3. Conventional machining program

Generally, cutting machines, including diamond turning lathes, are controlled by a machining program called NC code, which specializes in machine operations [38,39]. In the NC code, a program that commands the rotation speed and starting point, called PROLOG, is first read. Machining is then performed by referring to the coordinate values and moving each axis of the machine to the specified location. Therefore, the machined surface is defined using the coordinate point cloud data in the NC code.

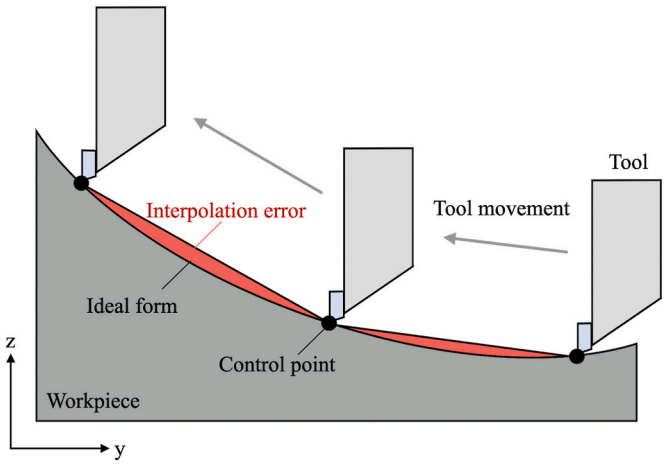

Fig. 5. Schematic of the interpolation error caused by moving a tool along the control points of a machining program.

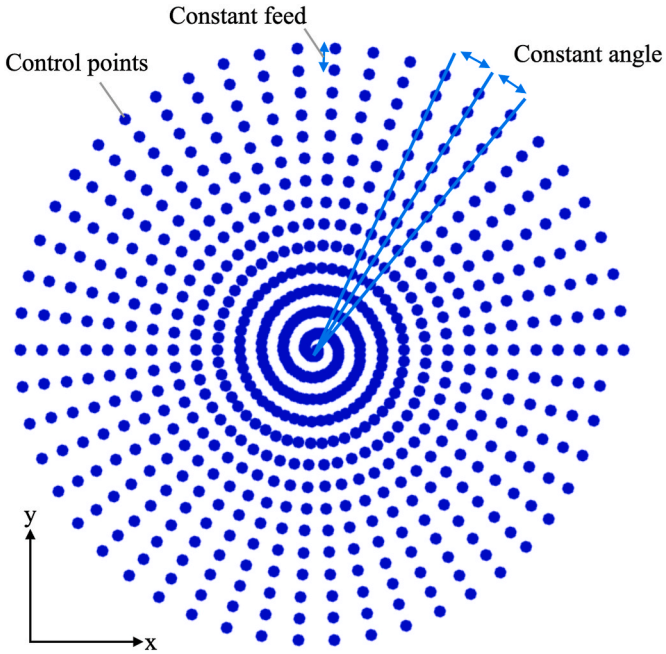

Fig. 6. Constant angle arrangement method for the point cloud data in a machining program.

This control method using the point cloud data of the NC code typically causes a problem called an interpolation error, as shown in Fig. 5 [27,40]. This error arises from the difference between the tool movement path and the ideal surface trajectory and affects the form error of the machined surface. The number of control points must be increased to suppress the form error caused by interpolation errors. However, the number of point cloud data points is limited depending on the machine, for example, up to one million points. Various studies on diamond turning, particularly on point cloud placement methods, have been conducted to achieve precision machining of freeform surfaces with a limited number of control points [25–27]. However, the standard constant-angle placement method shown in Fig. 6 is commonly used in machining programs for diamond turning [17,22,41].

This constant-angle arrangement method has the disadvantage that

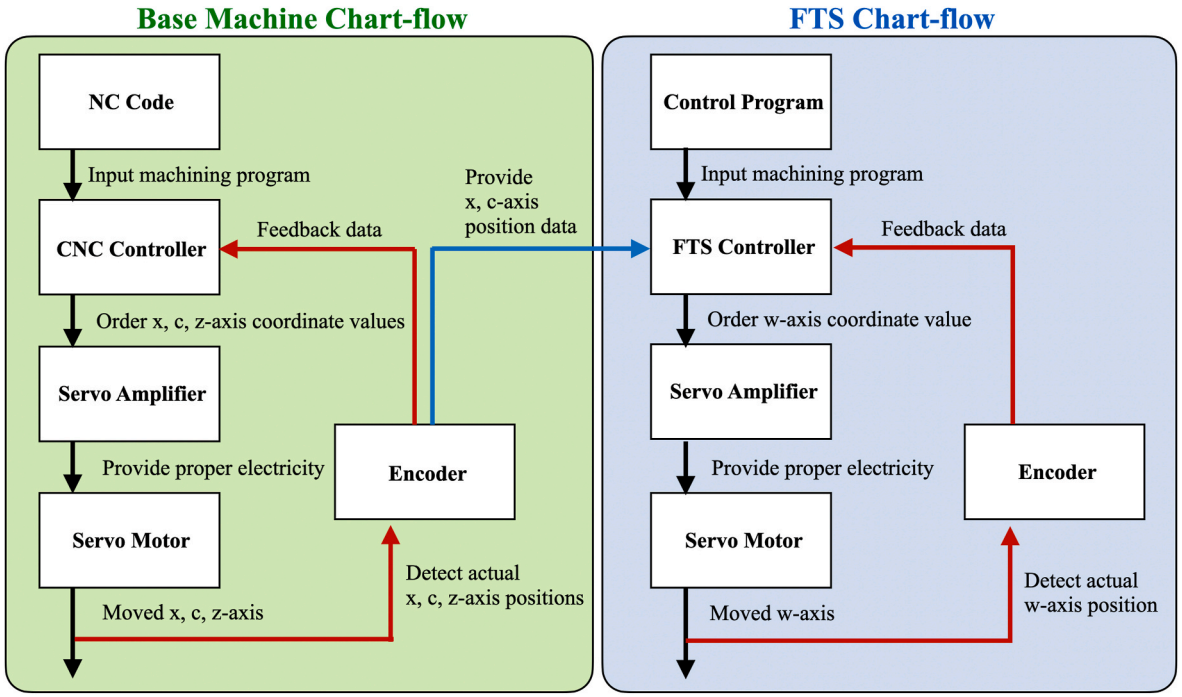

Fig. 7. Control chart-flow of diamond turning base machine and FTS unit specialized in tool movement in a single direction.

larger interpolation errors occur in the outer regions than in the inner regions of the workpiece. Although this effect was small for the machining of small-diameter lenses, the demand for machining large-diameter surfaces has been growing in recent years; a large out-of-tolerance interpolation error occurs on the machined surface when using a machining program with a limited number of point cloud data points. Regardless of the point cloud arrangement method used, as long as the ideal shape is defined by a point cloud, the larger the lens size, the larger the lens, the larger the interpolation error caused by point cloud limitations. Therefore, finding a method to overcome point cloud limitations for the machining of large optical freeform surfaces is imperative.

2.4. *Independently controlled FTS*

Independently controlled FTS, which has been developed in recent years, is equipped with a control system that specializes in the forward and backward motion of the axis in only one direction [17,18]. During machining, the coordinate information of the x- and c-axes of the base turning lathe is read from the encoder, and the FTS machining program calculates the tool position of the w-axis from this input data. The FTS control system then moves and controls the tool to the calculated position, as shown in Fig. 7. Specializing in controlling only the w-axis enables high-speed and high-precision movements. The machining program of this FTS does not require a conventional machining program (NC code) because it only requires information on the w-axis value of the tool position corresponding to the coordinate data of the base machine movement. Therefore, other programming languages, such as C, can be

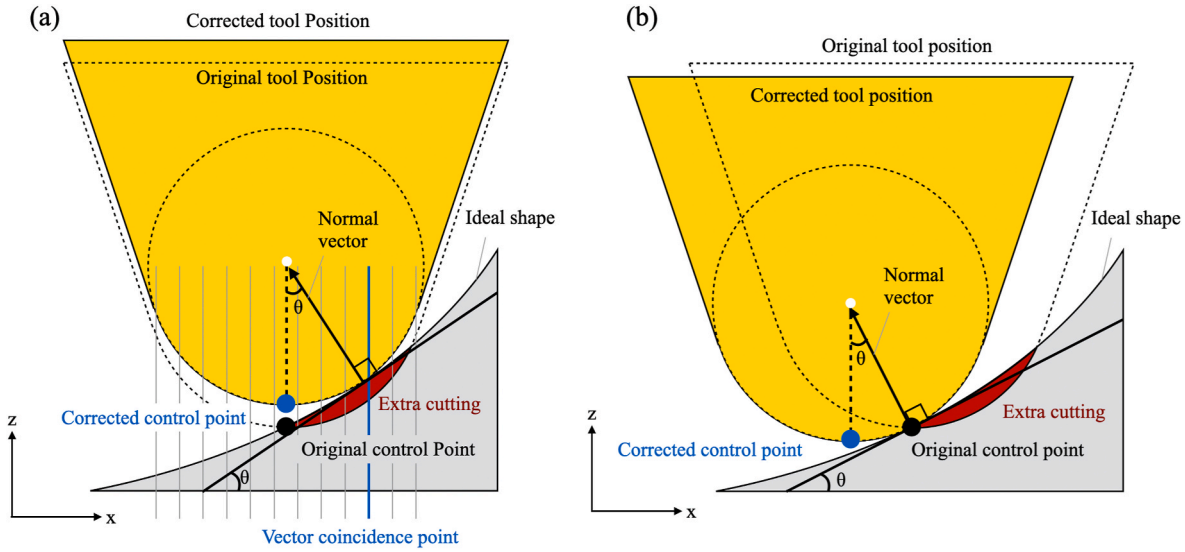

Fig. 8. Diagram of tool radius compensation by moving along (a) only the z-axis direction and (b) both the x- and z-axes directions.

used to control this FTS unit [42,43].

However, even for an independently controlled FTS with the aforementioned features, defining the design surface using point cloud data is considered the standard method in FTS machining [27,42]. The main reason for adopting point cloud data is the complexity of the tool radius compensation calculation. If the tool is V-shaped, the ideal surface can be machined by calculating the optical equation based on the designed coefficients during machining and moving the tool to the calculated position. However, because a V-shaped tool always contacts only a single point at its tip during machining, they wear out quickly. Therefore, a tool with a rounded tip is typically used in the diamond turning [12,23,24]. This round-nosed tool requires compensation for the ideal surface position according to the tool radius. In conventional point cloud-based machining, tool radius compensation is performed by calculating the compensation amount from the tool dimensions for each control point. To apply this tool radius compensation method to FTS machining, the surface is defined using point cloud data in the machining program of independently controlled FTS, even though it is possible to control the machine without point cloud data.

2.5. Proposed programming method

This study proposes a machining program that compensates the coefficients of the ideal surface design equation and evaluates these coefficients during machining, taking advantage of the control characteristics of the independent control system and machining program of the FTS.

First, a freeform surface was designed using an XY polynomial equation. Subsequently, the coefficients of the polynomial equation were corrected by applying the tool radius compensation method described in the following section. During machining, the FTS calculated the w-axis value of the ideal tool position based on the XY polynomial equation using the corrected coefficients, and then, moved the tool to the calculated w-axis position. Thus, the proposed method achieves higher-precision machining with smaller interpolation errors than a conventional point cloud-based machining program, while requiring a smaller data volume.

2.6. Tool radius compensation

Generally, tool radius compensation for a machining program with point cloud data is conducted by moving each control points only in the z-axis direction by calculating the compensation amount, as shown in Fig. 8(a) [22,39]. If the control point can be corrected in both the x- and z-axis directions, the compensation amount can be calculated using this approach because it can be treated as a linear problem, as shown in Fig. 8(b). In this method, the normal vector at each control point is calculated from the ideal surface, and the compensation amounts for the x- and z-axes are determined based on the tool radius. However, this compensation method of moving the control points in both the x- and z-axes direction makes it difficult to control the machine movement. The independently controlled FTS is a specialized machine for moving the tool only in the w-axis direction, which is in the same direction as the z-axis, and machining is conducted under high-speed rotation conditions to realize fast machining. If the control point is corrected in the x-axis direction, the main turning machine must control the x-axis during high-speed rotation. To avoid this problem, tool radius compensation focusing only on the z-axis direction is commonly used in FTS machining. However, calculating the correction amount using this compensation method requires solving a nonlinear problem, and finding the optimal value is time-consuming. This optimization must be conducted individually for each control point. A tradeoff exists: the more control points, the more precise the machining with smaller interpolation errors; however, the time required for tool radius compensation increases accordingly.

The compensation method in both the x- and z-axis directions is effective for correcting the ideal surface. The problem with this method is that the corrected point cloud data are treated as control points of the machining program, and the machine is moved to these control points. However, points corrected by moving in both the x- and z-axis directions can instead be used to compensate the coefficients of the XY polynomial equation. Specifically, first, point cloud data exceeding the maximum number of points readable by the machining program were first generated. Then, the correction amount in the x- and z-axis directions was calculated. Finally, the corrected coefficient values were computed by fitting the corrected point cloud to the XY polynomial equation. With this compensation method, even if the number of point cloud data points was increased, the time required for tool radius compensation was shorter than with the conventional z-axis-only method. As the corrected points themselves were not used in the actual control points of the machining program, the limitation on the number of point cloud data points in the machining program is no longer a concern. The original definition of the ideal shape is an XY polynomial, and the overall shape does not change significantly when tool radius compensation is applied. Therefore, only a minute change in the coefficient values from those of the original design equation was assumed, and the fitting error was expected to be small.

2.7. Fitting method based on XY polynomial equation

In this study, coefficient compensation was calculated by fitting the XY polynomial equation to the corrected point cloud data according to the tool radius. This section presents a method for calculating the best-fit coefficients of the XY polynomial from point cloud data of the freeform surface expressed on the x-, y-, and z-axes. When the XY polynomial expressed in Equation (2-a) is written in matrix form, the following equation is obtained:

$$\begin{bmatrix} {x_1}^{m_0}{y_1}^{n_0} & {x_1}^{m_1}{y_1}^{n_1} & \cdots & {x_1}^{m_{imax}}{y_1}^{n_{imax}} \\ {x_2}^{m_0}{y_2}^{n_0} & {x_2}^{m_1}{y_2}^{n_1} & \cdots & {x_2}^{m_{imax}}{y_2}^{n_{imax}} \\ \vdots & \vdots & \ddots & \vdots \\ {x_h}^{m_0}{y_h}^{n_0} & {x_h}^{m_1}{y_h}^{n_1} & \cdots & {x_h}^{m_{imax}}{y_h}^{n_{imax}} \end{bmatrix} \begin{bmatrix} C_0 \\ C_1 \\ \vdots \\ C_{i_{max}} \end{bmatrix} = \begin{bmatrix} z_1 \\ z_2 \\ \vdots \\ z_h \end{bmatrix}, \tag{4-a}$$

$$m_i = f_i - n_i, \tag{4-b}$$

$$n_i = i - \frac{f_i(f_i+1)}{2}, \tag{4-c}$$

$$f_i = \left\lfloor \frac{\sqrt{8i+1}-1}{2} \right\rfloor, \tag{4-d}$$

where h is the number of points in the point cloud data, and a floor function is used for f_i. The freeform surface of the XY polynomial can be determined using the above equations. If point cloud data of x-, y-, and z-axis values are available, the coefficient values of the XY polynomial can be calculated using the following equation:

$$\begin{bmatrix} C_0{}' \\ C_1{}' \\ \vdots \\ C_i{}' \end{bmatrix} = \begin{bmatrix} {X_1}^{m_0}{Y_1}^{n_0} & {X_1}^{m_1}{Y_1}^{n_1} & \cdots & {X_1}^{m_{imax}}{Y_1}^{n_{imax}} \\ {X_2}^{m_0}{Y_2}^{n_0} & {X_2}^{m_1}{Y_2}^{n_1} & \cdots & {X_2}^{m_{imax}}{Y_2}^{n_{imax}} \\ \vdots & \vdots & \ddots & \vdots \\ {X_h}^{m_0}{Y_h}^{n_0} & {X_h}^{m_1}{Y_h}^{n_1} & \cdots & {X_h}^{m_{imax}}{Y_h}^{n_{imax}} \end{bmatrix}^{-1} \begin{bmatrix} z_1 \\ z_2 \\ \vdots \\ z_h \end{bmatrix}, \tag{5-a}$$

$$X = \frac{x}{\max(|x|)}, \tag{5-b}$$

$$Y = \frac{y}{\max(|y|)}, \tag{5-c}$$

$$C_i = \frac{C_i{}'}{\max(|x|)^{m_i} \times \max(|y|)^{n_i}}. \tag{5-d}$$

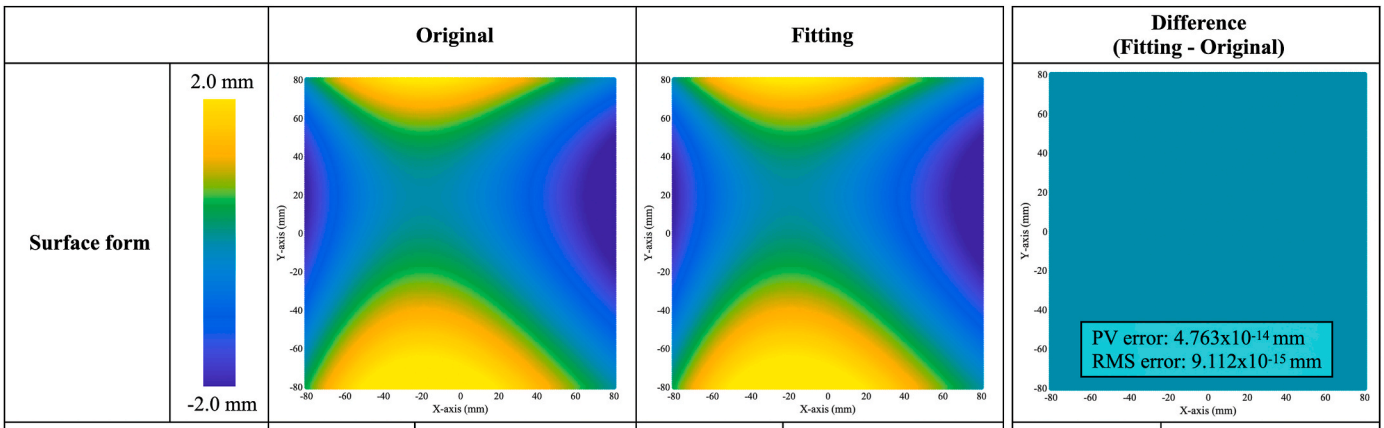

Coefficient	Original		Fitting		Difference (Fitting - Original)	
	$C_1\,(m=1, n=0)$	-0.014890738460	$C_1\,(m=1, n=0)$	-0.014890738460	$C_1\,(m=1, n=0)$	0.000000000000
	$C_2\,(0, 1)$	-0.014890738460	$C_2\,(0, 1)$	-0.014890738460	$C_2\,(0, 1)$	0.000000000000
	$C_3\,(2, 0)$	-0.000333333214	$C_3\,(2, 0)$	-0.000333333214	$C_3\,(2, 0)$	0.000000000000
	$C_5\,(0, 2)$	0.000333333214	$C_5\,(0, 2)$	0.000333333214	$C_5\,(0, 2)$	0.000000000000
	$C_6\,(3, 0)$	0.000001878192	$C_6\,(3, 0)$	0.000001878192	$C_6\,(3, 0)$	0.000000000000
	$C_9\,(0, 3)$	0.000001878192	$C_9\,(0, 3)$	0.000001878192	$C_9\,(0, 3)$	0.000000000000
	$C_{10}\,(4, 0)$	-0.000000000037	$C_{10}\,(4, 0)$	-0.000000000037	$C_{10}\,(4, 0)$	0.000000000000
	$C_{14}\,(0, 4)$	0.000000000037	$C_{14}\,(0, 4)$	0.000000000037	$C_{14}\,(0, 4)$	0.000000000000

Fig. 9. Example of an XY polynomial fitting result for a freeform surface obtained using the proposed fitting method.

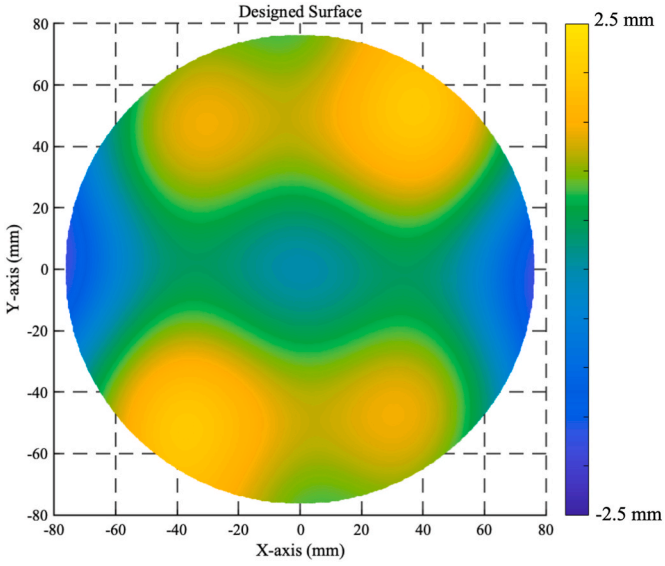

Fig. 10. Designed freeform surface defined by the XY polynomial for the cutting experiments.

Equation (5-a) utilizes the inverse matrix of Equation (4-a), with normalized values used for the x- and y-axes. When calculating the inverse matrix, the Moore–Penrose pseudoinverse, which can be calculated using the 'pinv()' function in MATLAB. The result of Equation (5-a) gives the coefficient of the surface with normalized x- and y-axis scales. To obtain the correct fitting coefficients, the normalized coefficients must be converted back to the original surface scale using Equation (5-d).

Coordinate normalization is introduced to improve the numerical conditioning of the regression matrix. Without normalization, the powers of the original coordinates can lead to large differences in magnitude among the matrix elements, particularly for higher-order polynomial terms. This results in an ill-conditioned system, where small numerical errors can be amplified during the computation of the pseudoinverse. By scaling the coordinates to a comparable range prior to constructing the regression matrix, the magnitude of each basis term is balanced, which reduces the condition number of the matrix. As a result, the coefficient estimation becomes more stable and less sensitive to numerical errors, even in the presence of measurement noise and higher-order polynomial terms.

Table 2
Coefficients of the designed freeform surface defined by the XY polynomial.

$C_0\,(m=0, n=0)$	−0.029065634279
$C_3\,(2, 0)$	0.000854545700
$C_4\,(1, 1)$	0.000160696902
$C_5\,(0, 2)$	0.001329701256
$C_{10}\,(4, 0)$	−0.000000491886
$C_{11}\,(3, 1)$	0.000000000002
$C_{12}\,(2, 2)$	−0.000000000010
$C_{13}\,(1, 3)$	0.000000000018
$C_{14}\,(0, 4)$	−0.000000491824
$C_{21}\,(6, 0)$	0.000000000078
$C_{27}\,(0, 6)$	0.000000000078

A comparison between the freeform surfaces calculated using the original and fitted coefficients was conducted to evaluate the accuracy of the fitting method for the XY polynomial equation. The evaluation results are shown in Fig. 9. The results show that the errors between the original and fitted coefficients errors were less than 10^{-12} for each coefficient and the PV error between the two surfaces was the 4.763×10^{-14} mm, confirming that the fitting was performed with extremely high accuracy.

3. Experimental demonstration

3.1. Designing of freeform surface

The designed freeform surface and its coefficients are presented in Fig. 10 and Table 2, respectively. The interpolation error of a machining program based on point cloud data increases when machining larger

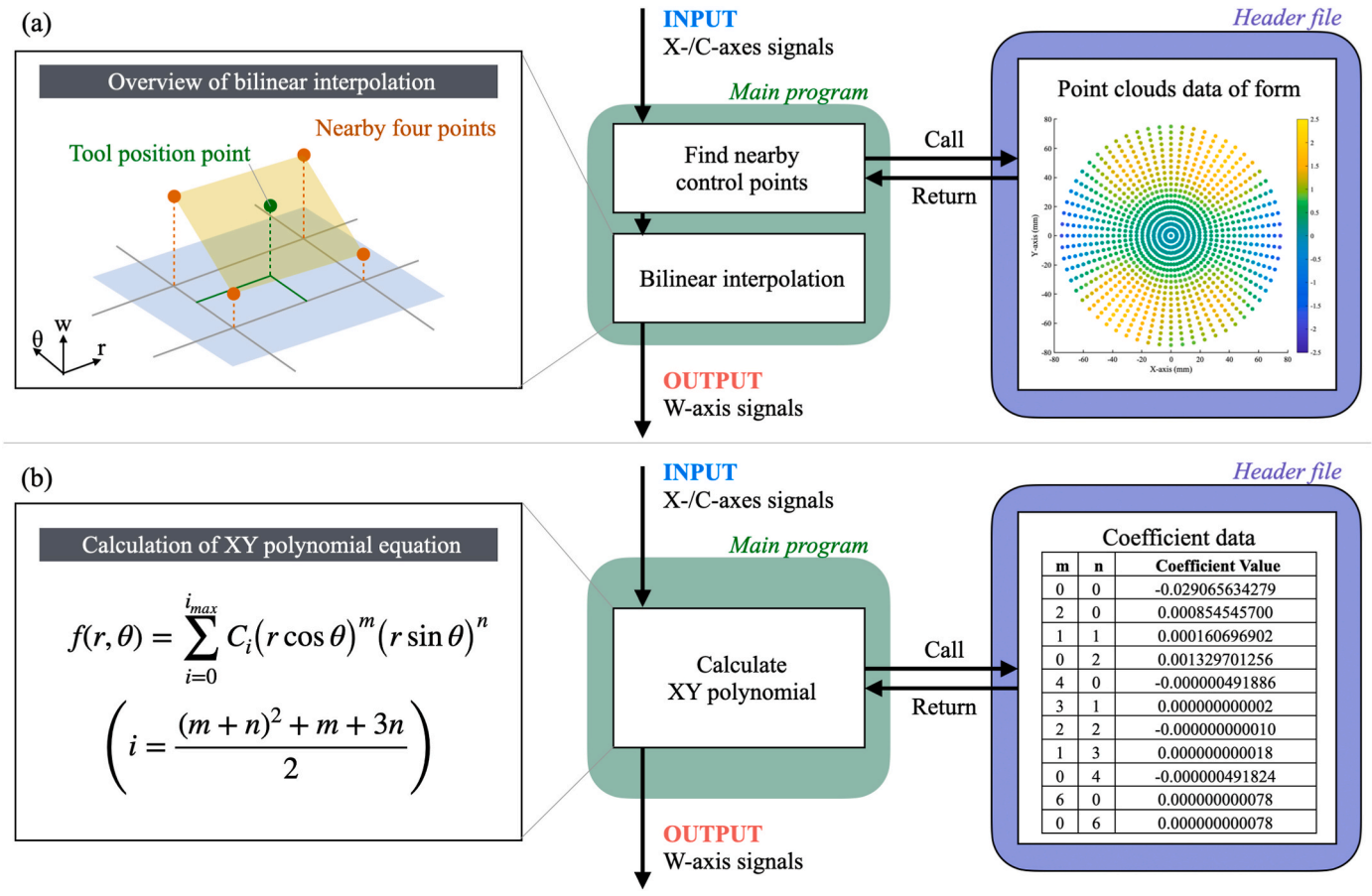

Fig. 11. Schematic of w-axis value calculation performed by (a) the conventional machining program based on bilinear interpolation using point cloud data and (b) the proposed novel machining program using coefficient data.

workpieces because the number of point cloud data points remains limited. To check the effectiveness of the proposed machining program, the diameter of the designed freeform surface was decided to be as large as possible; ϕ150 mm was selected by considering the load capacity of the spindle of turning lathe used in this study and potential interference during machining. In addition, because the FTS used in this experiment had a stroke limit of 5 mm, the freeform surface was designed such that the height variation of the machined surface remained within 5 mm.

3.2. Machining program

A conventional machining program using point cloud data and the

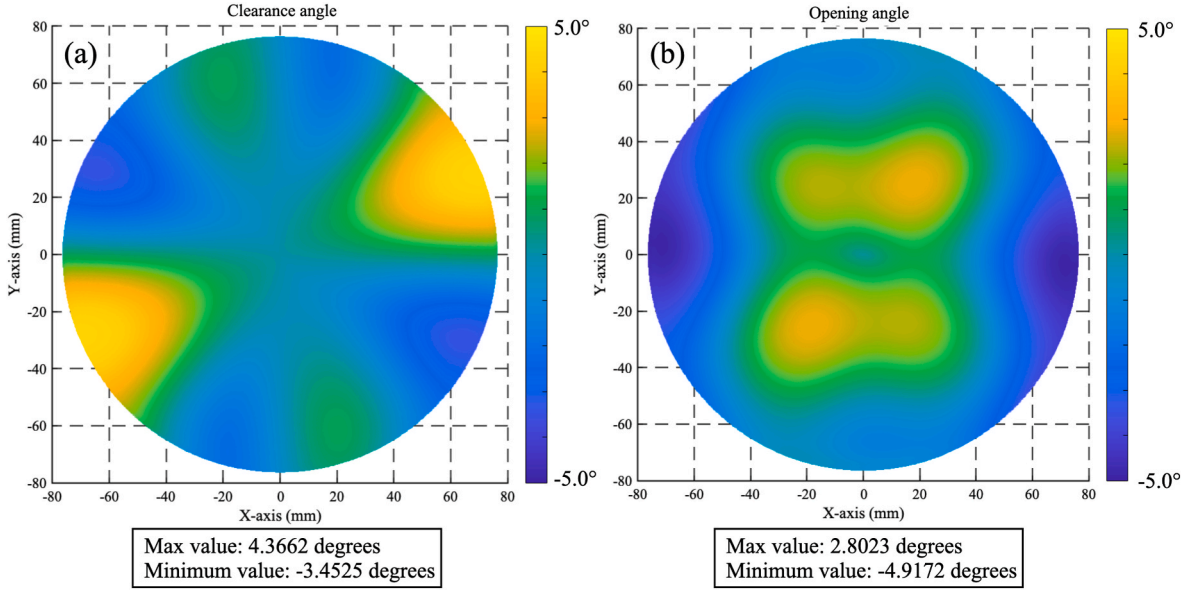

Fig. 12. Calculation results of required (a) clearance angle and (b) opening angle for a round-nosed diamond tool.

Table 3
Specifications of the diamond tools used in the cutting experiments.

Tool material	Single-crystal diamond
Nose radius (mm)	1.013
Rake angle (°)	0
Clearance angle (°)	15
Open angle (°)	120

proposed machining program using coefficient data were prepared for an FTS cutting experiment mounted on a diamond turning lathe. The workflow of both machining programs is shown in Fig. 11.

In the conventional machining program using point cloud data, an interpolation process was conducted to calculate the w-axis value of the tool position based on the input x- and c-axis information from the base machine, as shown in Fig. 11(a). A bilinear interpolation method, which is commonly used in FTS machining programs, was applied to the conventional point cloud machining program [17,42]. The interpolation method identified the four nearest points of the input base machine coordinates and calculated the corresponding w-axis value. For the arrangement of the point cloud data, the constant angle method, which is the standard arrangement method described in Section 2.3, was adopted; the constant angle and pitch were 0.5° and 0.058 mm, respectively. The total number of point cloud data points was 993,600, which is close to the upper limit of one million points of the FTS used in this study.

In the proposed machining program using coefficient data, only 20 coefficient values were required, and the machining program evaluated the XY polynomial equation based on these coefficient values and the input coordinate information from the base machine, as shown in Fig. 11 (b). This represents a reduction in the number of representation parameters to approximately 1/50,000 compared to the 993,600 data points used in the conventional method.

3.3. Experimental setup

To determine suitable diamond tool specifications for machining the ideal surface without interference, each normal vector of the x- and c-axes were calculated from the designed freeform surface, as shown in Fig. 12. From these calculations, the diamond tool was required to have an opening angle of at least 4.917° and a clearance angle of at least 3.453°. The tools listed in Table 3 were selected to satisfy these specifications.

To machine the designed freeform surface, diamond turning was performed using a fast tool servo FTS-5000 (AMETEK Precitech Inc.) mounted on an ultraprecision Nanoform X (AMETEK Precitech Inc.), as shown in Fig. 13. To realize precise machining using the FTS, the spindle rotation speed was carefully determined, such that the tool acceleration did not exceed the maximum acceleration specified for the FTS, and the rotation speed was set to 100 rpm. The sampling frequency of the FTS was 20 kHz, and the typical computation time per control cycle was 383 μs. This computation delay was compensated using the built-in time-delay compensation function of the FTS by pre-calculating the angular shift caused by the delay [17,18]. All cutting parameters used in this experiment are summarized in Table 4. Aluminum, which has high machinability and reduce the weight of large-diameter workpieces, was

Table 4
Experimental conditions.

Cutting Parameters	
Depth of cut (μm)	Rough: 10 Finish: 2
Spindle rotation rate (rpm)	100
Feed rate (μm/rev)	0.5
Workpiece	
Material	Aluminum
Diameter (mm)	170
Cutting area diameter (mm)	150

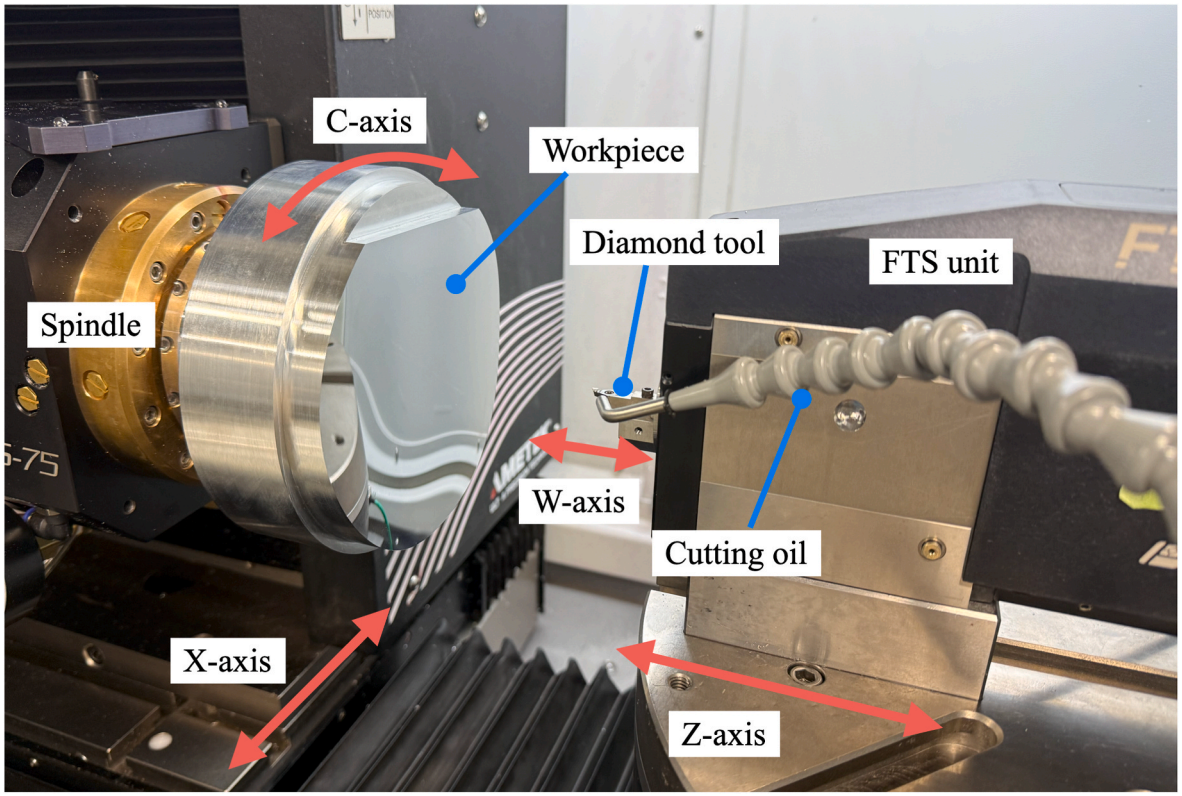

Fig. 13. Photograph of the main section of the FTS-based diamond turning experimental setup.

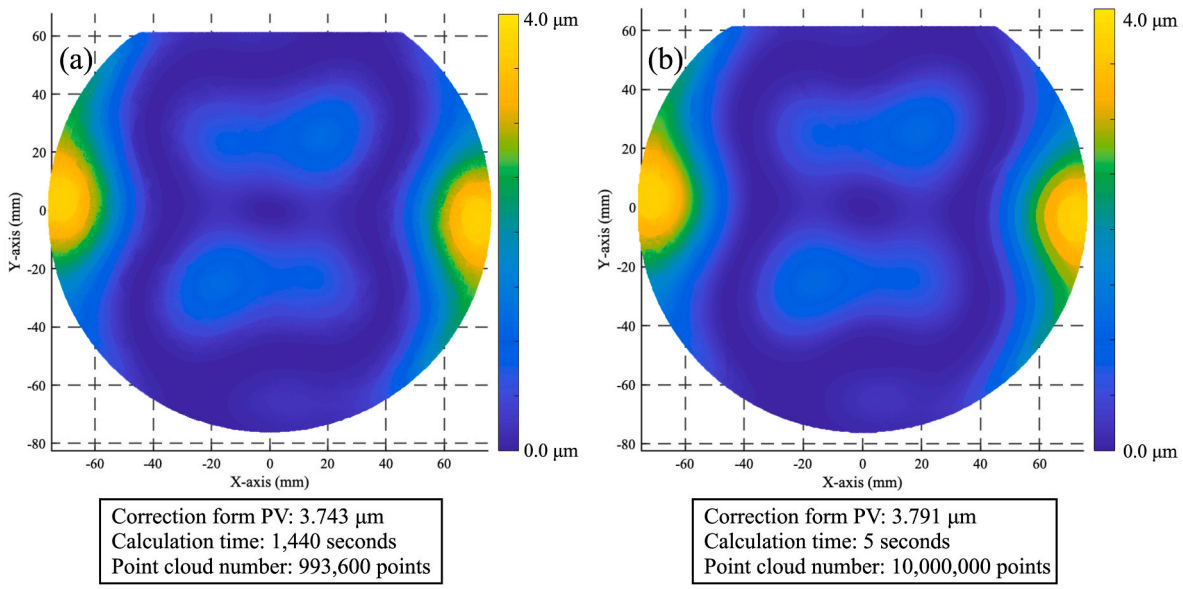

Fig. 14. Calculated correction surfaces for (a) the conventional machining program and (b) the proposed machining program.

selected as the workpiece material. The same designed freeform surface was machined using the two machining programs described in Section 3.2 under the above machining conditions. White-light interferometry Nexview2 (AMETEK Zygo Corp.) was used to measure the machined surfaces using a 50× objective lens with a measurement area of 1 mm × 1 mm. Since the evaluated region exceeded a single field of view, multiple measurements were stitched together to obtain the full surface data. After obtaining the measurement data, the form error of the machined surfaces was analyzed by best fitting the acquired data to the ideal surface form in MATLAB. No filtering or post-processing smoothing was applied to the raw measurement data prior to form error evaluation.

3.4. Tool radius compensation results

Tool radius compensation was conducted on the designed freeform surface for both machining programs. The calculated correction surface is illustrated in Fig. 14.

For the tool radius compensation of the conventional machining program using point cloud data, the correction amount in only the z-axis direction was calculated by nonlinear regression because the corrected point cloud data were directly used as control points of machining program. The calculated results are presented in Fig. 14(a). Comparing these results with the normal angle distribution in the radial direction in Fig. 12(b), the correction amount and the normal angle in the radial direction were correlated, and the correction amount was larger when the absolute value of the vertical angle was larger. The form PV value of this correction surface was 3.743 µm. As described in Section 2.6, calculating the tool radius compensation along the ideal surface in the z-axis direction only requires solving an optimization calculation for each control point, which result in a long calculation time. The calculation of the correction for the conventional machining program required 1440 s.

The tool radius compensation for the proposed machining program with coefficient data was conducted by calculating the correction amount in both the x- and z-axis directions as a linear regression problem. No limitation exists on the number of point cloud data points for an ideal freeform surface because the point cloud data are not treated as control points for the machining program. In this study, 10 million data points, which is 10 times the control-point limit, were prepared to calculate the correction for the proposed machining program. The calculated results are presented in Fig. 14(b). Even when corrections in both the x- and z-axes direction were applied to the tool radius compensation, the resulting correction surface geometry was identical to that of the conventional method, as shown in Fig. 14(a) and (b). The PV value of this correction surface was 3.791 µm, and the calculation time was less than 5 s, representing a reduction of more than 99.9% compared with that of the conventional machining program, owing to the use of linear regression.

Table 5
Coefficients of the correction surface and the combined surface.

	Correction surface	Combined surface (Design + Correction)
C_0 ($m=0$, $n=0$)	0.000009119762	−0.029056514517
C_1 (1, 0)	0.000000071762	−0.000000071762
C_2 (0, 1)	−0.000000067910	−0.000000067910
C_3 (2, 0)	0.000001441123	0.000855986823
C_4 (1, 1)	0.00000652206	0.000161349108
C_5 (0, 2)	0.00003260607	0.001332961863
C_6 (3, 0)	−0.00000000151	−0.00000000151
C_7 (2, 1)	−0.00000001523	−0.00000001523
C_8 (1, 2)	−0.00000000538	−0.00000000538
C_9 (0, 3)	−0.00000000972	−0.00000000972
C_{10} (4, 0)	−0.000000003233	−0.000000495119
C_{11} (3, 1)	−0.00000000573	−0.00000000571
C_{12} (2, 2)	−0.00000001367	−0.00000001377
C_{13} (1, 3)	0.00000000105	0.00000000123
C_{14} (0, 4)	0.00000003897	−0.000000495721
C_{18} (2, 3)	−0.00000000004	−0.00000000004
C_{20} (0, 5)	0.00000000005	0.00000000005
C_{21} (6, 0)	0.00000000002	0.00000000080
C_{23} (4, 2)	−0.00000000001	−0.00000000001
C_{27} (0, 6)	0.00000000001	0.00000000079

Based on the calculated correction surface in Fig. 14(b), the coefficient values were compensated by applying the fitting method described in Section 2.7. The fitted coefficient values and fitting errors are presented in Table 5 and Fig. 15, respectively. The PV value of the fitting error was 0.096 µm. The fitting calculation time was less than 5 s because this calculation was solved as a linear regression problem. The fitting coefficient values were treated as the corrected coefficients of the proposed machining program, and the XY polynomial equation was evaluated based on these corrected coefficient values during machining.

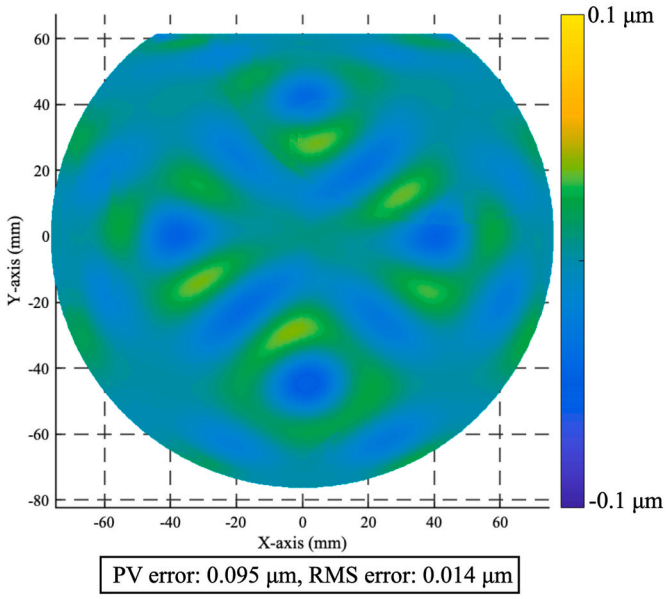

Fig. 15. Fitting error when fitting the XY polynomial to the correction surface shown in Fig. 14(b).

3.5. Surface topography results

The designed freeform surface was machined using a conventional machining program based on the bilinear interpolation method and the proposed machining program that directly evaluates the XY polynomial equation. Images of the machined surfaces are shown in Fig. 16. When the outer edge of the machined surface was examined at higher magnification radial patterns were observed on the surface machined using the conventional machining program, as shown in Fig. 16(b). This pattern corresponds to the constant-angle point cloud arrangement method, and it is believed that the characteristic form error pattern caused by interpolation errors manifests as this visible pattern.

In contrast, the surface machined using the proposed method did not exhibit a radial pattern, as shown in Fig. 16(c). This is likely because the diamond tool moved in direct correspondence with the evaluated XY polynomial equation, realizing smooth tool motion consistent with the designed surface geometry. These observations indicate that the proposed machining program produces a superior surface appearance compared with the conventional bilinear interpolation method.

3.6. Form error evaluation

The surface geometry of each surface machined using the conventional and novel proposed machining programs was measured using a white-light interferometer, and the form errors between the measured and ideal surfaces were analyzed in MATLAB. The measurement areas and positions are illustrated in Fig. 17, and the form error evaluation results are shown in Fig. 18.

As shown in Fig. 18(a), characteristic radial form errors occurred on the surface machined using the conventional bilinear interpolation method. This radial form error pattern was caused by the interpolation error of the point cloud data in the conventional machining program. Even though the point cloud data comprised nearly one million points, close to the reading limit, this number of data points was insufficient for machining a freeform surface with a diameter of 150 mm. In contrast, significantly better form accuracy was obtained for the surface machined using the proposed machining program, as shown in Fig. 18

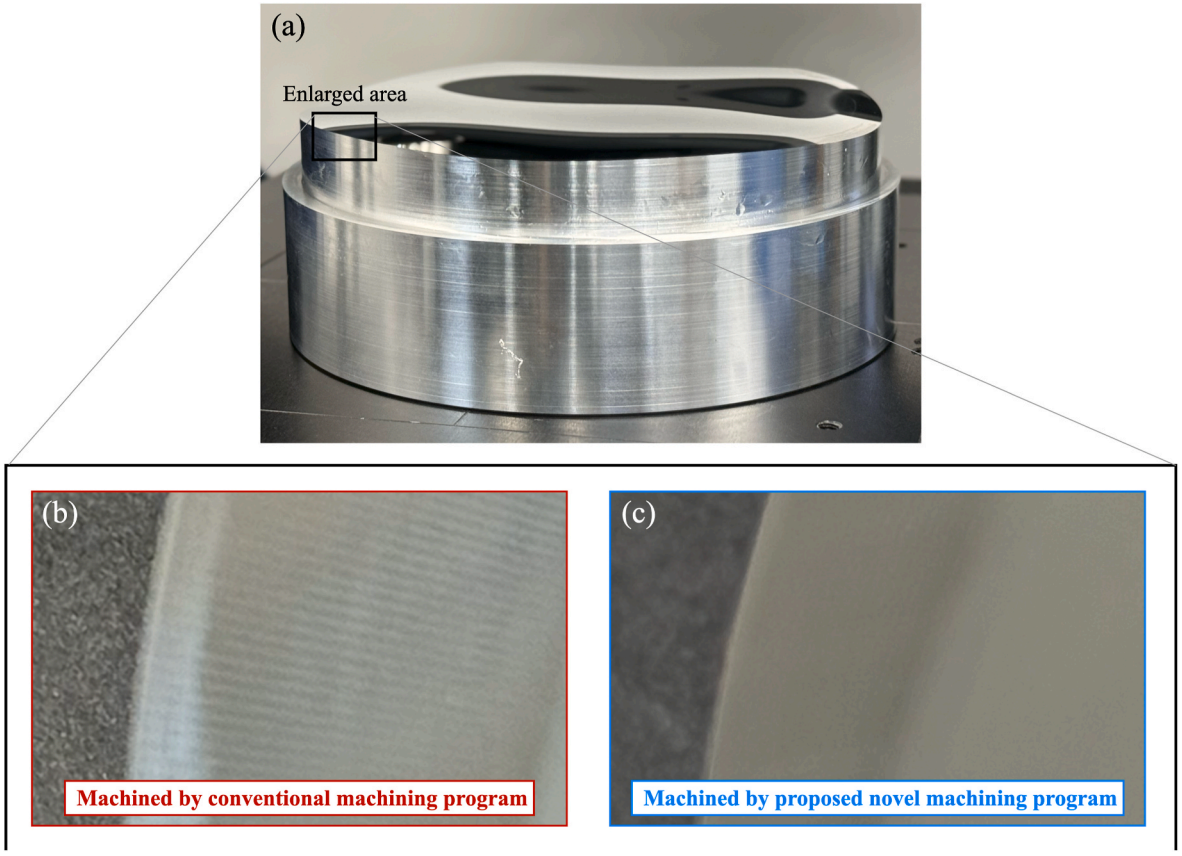

Fig. 16. Photograph of the machined surface: (a) overall surface appearance; enlarged view of the machined surface obtained using the (b) conventional machining program and (c) proposed machining program.

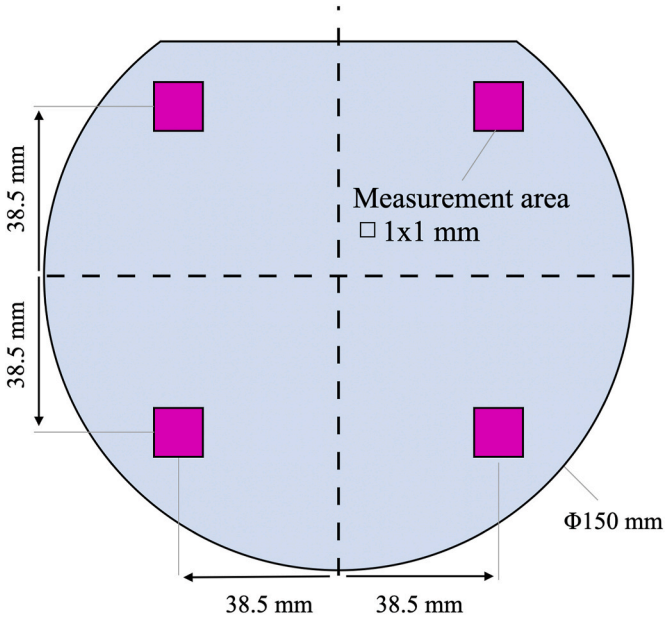

Fig. 17. Measurement areas and positions of single freeform surface machining.

(b). The maximum PV and RMS form errors obtained using the conventional and proposed machining programs were 0.399 and 0.037 μm, and 0.150 and 0.009 μm, respectively. These results indicate that the proposed method reduced the form errors by 62.4% and 75.7%, respectively, demonstrating the effectiveness of the proposed machining program.

To assess variability, four different locations on the machined surface were evaluated. The results for the proposed method, shown in Fig. 18 (b), exhibited limited variation, with PV values ranging from 0.106 to 0.150 μm and RMS values ranging from 0.006 to 0.009 μm across the measured areas. This indicates high consistency of the overall process, supported by the nanometer-scale positioning capability of the voice-coil-driven FTS and the nanometer-scale measurement resolution of the white-light interferometer.

4. Application to multi-surface machining

4.1. Design of multiple freeform surfaces

The proposed machining program has the potential to contribute to high-efficiency machining with high stability and accuracy. When performing multi-surface machining, even if each individual optical surface is small, the total machining area increases as the number of surfaces and the machining range radius increase. When attempting to achieve multi-surface machining using a conventional machining program with a limited number of points arranged in a constant-angle pattern, the outer surfaces would exhibit poorer machining accuracy than the inner surfaces due to the lower point cloud density at larger radii. Although conventional point cloud machining programs suffer from unstable accuracy in multi-surface machining, the proposed machining program has the potential to provide a new solution to this problem.

To verify the effectiveness of the proposed machining program for multi-surface machining, five similar optical surfaces with different elevation differences were designed using an XY polynomial equation. The coefficients of these design surfaces are listed in Table 6. Fig. 19 shows each designed optical surface and the arrangement of these surfaces during multi-surface machining via diamond turning. Surface 1 was positioned at the center of the machining area, and Surfaces 2, 3, 4, and 5 were positioned at the right, top, left, and bottom, respectively. Each optical surface in this arrangement was machined in a single setup on the diamond turning lathe.

4.2. Machining program

Multi-surface machining was conducted using both the conventional point cloud and proposed machining programs, as in the basic cutting experiment described in Section 3.2, to compare the results of each machining program. The workflow of the conventional machining

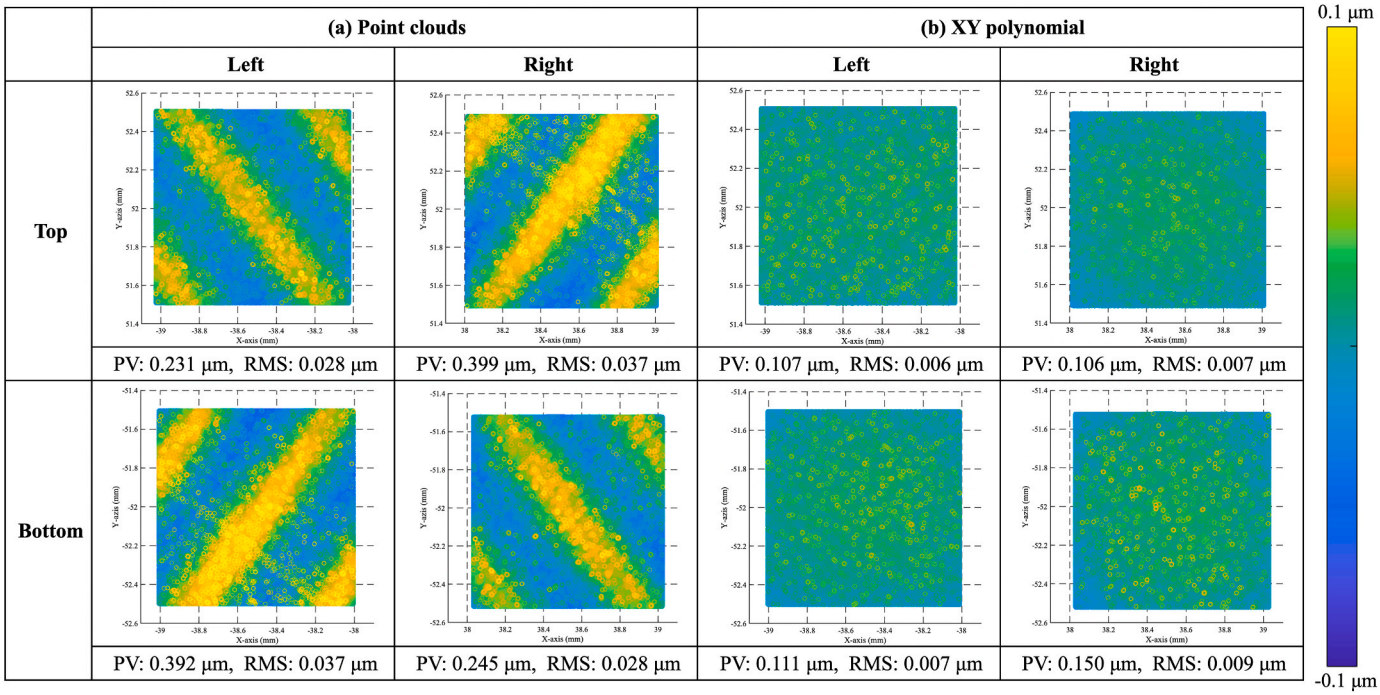

Fig. 18. Evaluated form error results at the locations shown in Fig. 17, obtained by best fitting the ideal surface to the measured data of the surfaces machined using the (a) conventional machining program with point cloud data and (b) proposed machining program with coefficient data.

Table 6
Coefficients of design surfaces for multi-surface machining.

	Surface1	Surface2	Surface3	Surface4	Surface5
C_0 ($m=0$, $n=0$)	−0.049933656541	−0.099997972241	−0.149996958027	−0.199995943410	−0.249994928258
C_2 (0, 1)	−0.004363119464	−0.004362457414	−0.004361340654	−0.004359777191	−0.004357767023
C_3 (2, 0)	0.001225437515	0.001096268285	0.001644402422	0.002192536552	0.002740670673
C_5 (0, 2)	0.001225460846	0.001096289147	0.001644433695	0.002192578214	0.002740722693
C_7 (2, 1)	−0.000000004826	−0.000000009029	−0.000000020315	−0.000000036115	−0.000000056429
C_9 (0, 3)	−0.000000005770	−0.000000014389	−0.000000032375	−0.000000057555	−0.000000089929
C_{10} (4, 0)	−0.000009820783	−0.000003994505	−0.000005991757	−0.000007989009	−0.000009986261
C_{12} (2, 2)	−0.000000000001	0.000000000000	0.000000000000	0.000000000001	0.000000000002
C_{14} (0, 4)	−0.000009821157	−0.000003994657	−0.000005991984	−0.000007989311	−0.000009986638
C_{16} (4, 1)	0.000000000016	0.000000000024	0.000000000054	0.000000000097	0.000000000151
C_{18} (2, 3)	0.000000000046	0.000000000051	0.000000000116	0.000000000207	0.000000000323
C_{20} (0, 5)	0.000000000047	0.000000000078	0.000000000177	0.000000000315	0.000000000493
C_{21} (6, 0)	0.000000028847	0.000000005670	0.000000008505	0.000000011340	0.000000014175
C_{27} (0, 6)	0.000000028849	0.000000005670	0.000000008505	0.000000011340	0.000000014176
C_{36} (8, 0)	−0.000000000033	−0.000000000004	−0.000000000006	−0.000000000008	−0.000000000009
C_{44} (0, 8)	−0.000000000033	−0.000000000004	−0.000000000006	−0.000000000008	−0.000000000009

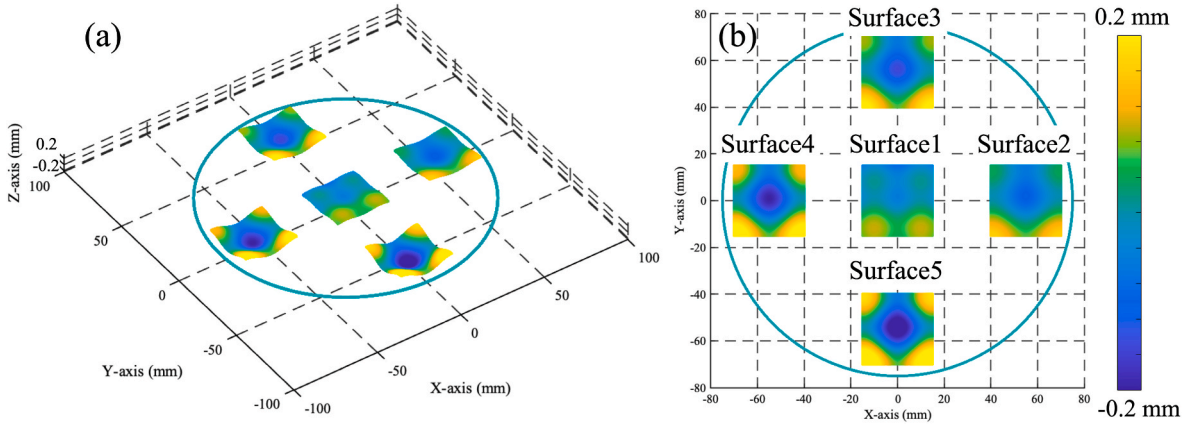

Fig. 19. (a) Overall view and (b) layout of the five freeform surfaces defined by the XY polynomial for multi-surface machining.

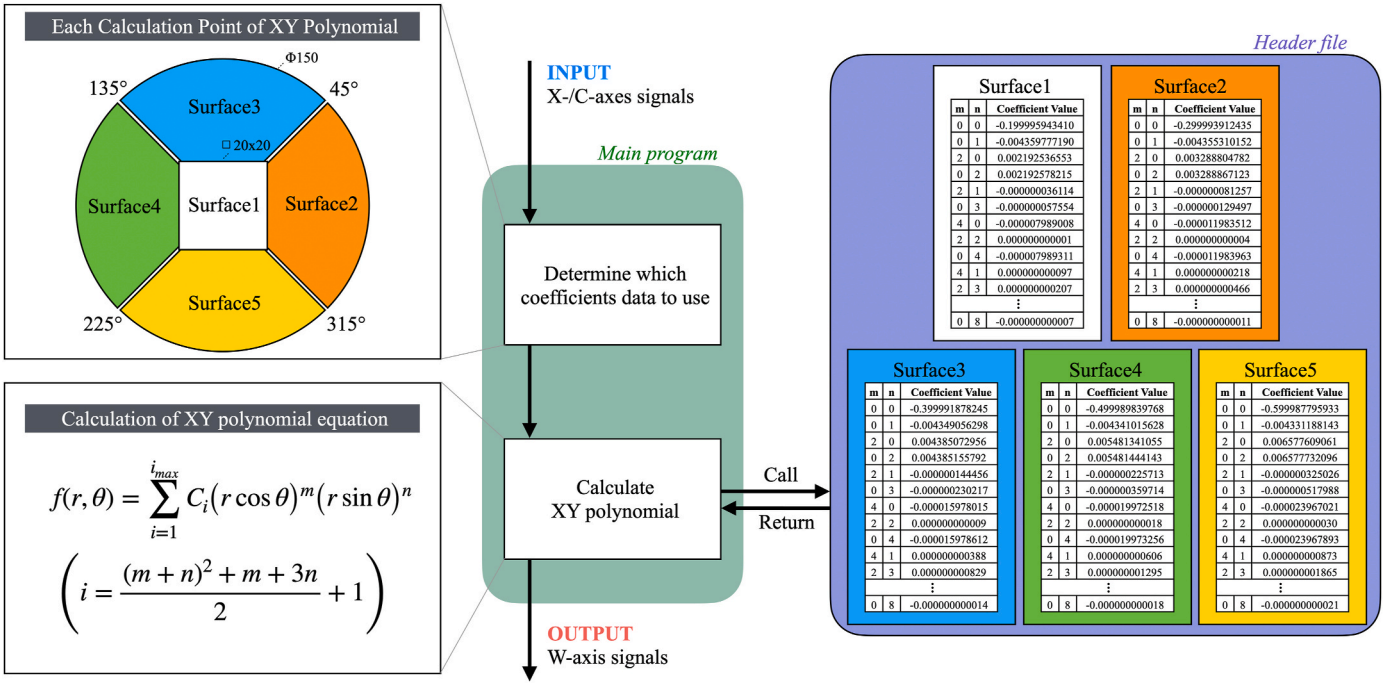

Fig. 20. Schematic of the w-axis value calculation of the proposed machining program using multiple coefficient datasets for the advanced cutting experiment.

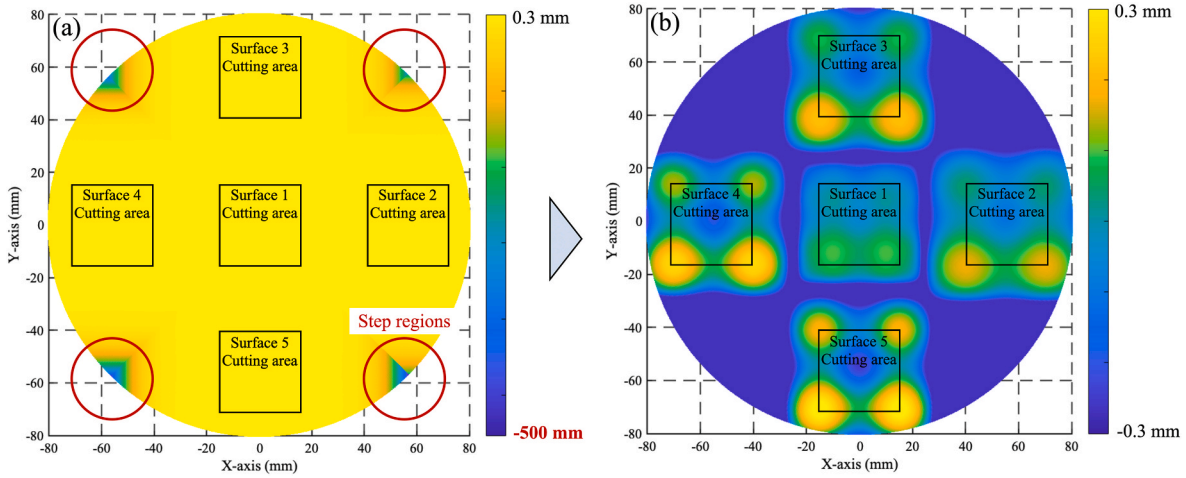

Fig. 21. Surface plot of the machining program output using cutting area data (a) before and (b) after applying the additional overwrite routine.

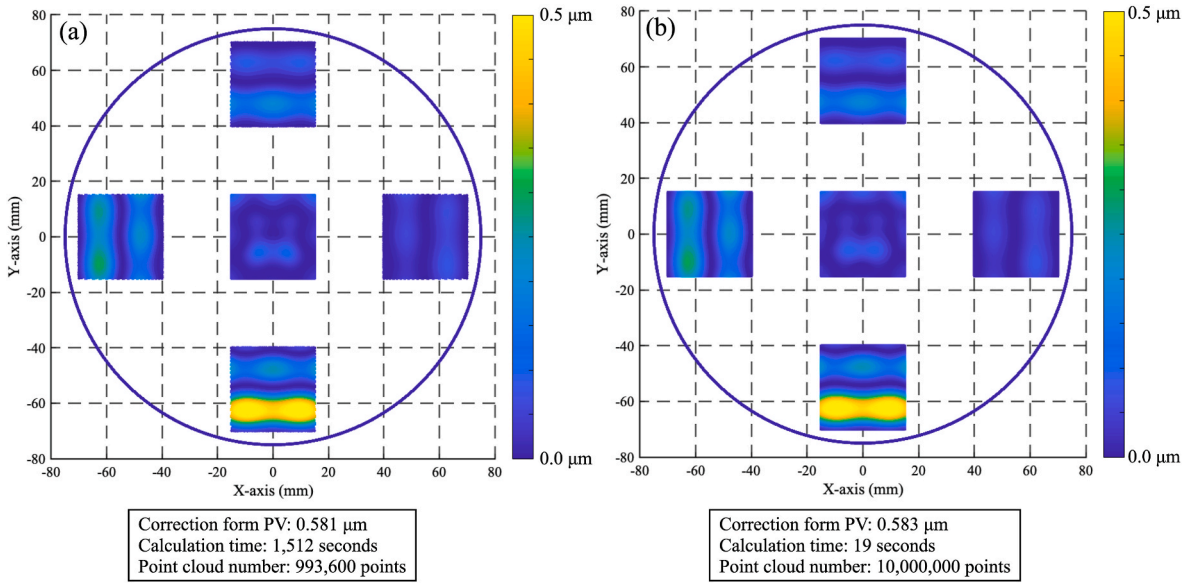

Fig. 22. Calculated correction surface for the (a) conventional machining program and (b) proposed machining program for multi-surfaces machining.

program using point cloud data is identical to that of the basic cutting experiment described in Section 3.2, as shown in Fig. 11(a). In contrast, the proposed machining program must handle the coefficients of the XY polynomial for five optical surfaces, unlike the workflow for single-surface machining. To realize multi-surface machining using the proposed machining program, a direct-calculation program was developed, as shown in Fig. 20. The key feature of this machining program is the selection of the appropriate optical surface coefficients based on the acquired x- and c-axis coordinate values. When the tool movement was controlled from the x- and c-axis coordinate values based on the workflow shown in Fig. 20, the XY polynomial produced a steep elevation difference as the tool moved away from the center position of each surface. Consequently, the tool was likely to follow this steep profile, as shown in Fig. 21(a), which exceeded the 5 mm stroke limit of the FTS and made smooth machining impossible. In addition, because the workpiece rotates during turning, a large step in tool motion occurred at the boundary where the coefficients switched between optical surfaces, making FTS control difficult. To solve these problems, a supplementary routine was added that constrained the w-axis value to −0.027 mm whenever the calculated w-axis value fell below −0.027 mm. By applying this additional routine, the FTS moved the tool smoothly, as shown in Fig. 21(b). This ensured smooth transitions without steps even outside the cutting area, reducing the control load on the FTS and enabling high-precision machining. The smooth connection profile between each optical surface was also used as the reference form for the point cloud data in the conventional machining program.

The XY polynomial direct-calculation machining program for multi-surface machining requires loading coefficients for each optical surface, resulting in five times the data volume compared with the basic cutting experiment described in Section 3. However, even with five times the amount of data, the total number of coefficients was only 330. Compared with the 993,600 points required by the point cloud machining program, this represents less than 0.04% of the point cloud data volume.

4.3. Tool radius compensation

Tool radius compensation was performed for both the conventional and proposed machining programs for multi-surface machining. The calculated correction surfaces are shown in Fig. 22. The conventional point cloud machining program, which required correcting points by moving only in the Z-axis direction, required 1510 s to process 993,600

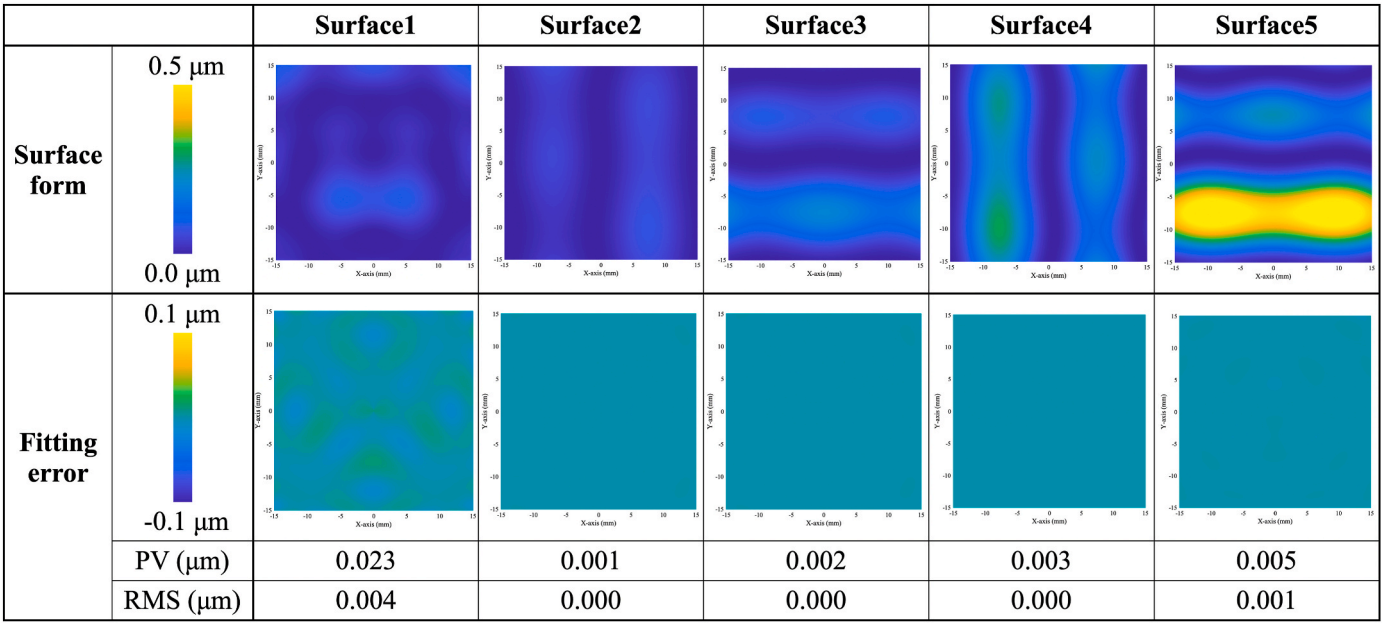

Fig. 23. Correction surfaces and fitting errors obtained when calculating the XY polynomial fitting coefficients for each surface.

Table 7
Fitted coefficients of correction surfaces for multi-surface machining.

	Surface1	Surface2	Surface3	Surface4	Surface5
C_0 ($m=0$, $n=0$)	−0.049924266524	−0.099997885062	−0.149987053353	−0.199995579603	−0.249984635490
C_1 (1, 0)	0.000000000000	0.000000063551	0.000000000000	−0.000000262422	0.000000000000
C_2 (0, 1)	−0.004373052655	−0.004362457088	−0.004375832465	−0.004359776892	−0.004382614955
C_3 (2, 0)	0.001227518549	0.001098696990	0.001644130623	0.002202267951	0.002741105039
C_4 (1, 1)	0.000000000000	−0.000000177290	0.000000000000	0.000000355217	0.000000000000
C_5 (0, 2)	0.001228069560	0.001096291182	0.001649902777	0.002192576961	0.002755940738
C_6 (3, 0)	0.000000000000	−0.000000000824	0.000000000000	0.000000003611	0.000000000000
C_7 (2, 1)	0.000000033396	−0.000000005848	0.000000173629	−0.000000029938	−0.000000552718
C_8 (1, 2)	0.000000000000	0.000000081714	0.000000000000	−0.000000327492	0.000000000000
C_9 (0, 3)	0.000000103539	−0.000000017631	0.000000073196	−0.000000064050	0.000000095963
C_{10} (4, 0)	−0.000009875886	−0.000004029366	−0.000005988121	−0.000008129002	−0.000009985182
C_{11} (3, 1)	0.000000000000	0.000000001242	0.000000000000	−0.000000002506	0.000000000000
C_{12} (2, 2)	−0.000000019225	−0.000000002117	−0.000000005028	−0.000000008486	−0.000000012865
C_{13} (1, 3)	0.000000000000	0.000000000175	0.000000000000	−0.000000000339	0.000000000000
C_{14} (0, 4)	−0.000009885278	−0.000003993942	−0.000006070581	−0.000007986456	−0.000010205812
C_{16} (4, 1)	0.000000001029	0.000000000002	−0.000000001277	0.000000000055	0.000000003671
C_{17} (3, 2)	0.000000000000	−0.000000000486	0.000000000000	0.000000001951	0.000000000000
C_{18} (2, 3)	−0.000000001573	0.000000000046	−0.000000001008	0.000000000197	0.000000003332
C_{19} (1, 4)	0.000000000000	−0.000000000573	0.000000000000	0.000000002295	0.000000000000
C_{20} (0, 5)	0.000000000161	0.000000000104	−0.000000000063	0.000000000366	0.000000000108
C_{21} (6, 0)	0.000000029317	0.000000005861	0.000000008480	0.000000012109	0.000000014127
C_{23} (4, 2)	0.000000000189	0.000000000018	0.000000000023	0.000000000072	0.000000000059
C_{25} (2, 4)	0.000000000228	0.000000000010	0.000000000042	0.000000000039	0.000000000111
C_{26} (1, 5)	0.000000000000	−0.000000000001	0.000000000000	0.000000000002	0.000000000000
C_{27} (0, 6)	0.000000029387	0.000000005661	0.000000008937	0.000000011305	0.000000015381
C_{29} (6, 1)	−0.000000000007	0.000000000000	0.000000000002	0.000000000000	−0.000000000007
C_{31} (4, 3)	0.000000000003	0.000000000000	0.000000000007	0.000000000000	−0.000000000020
C_{32} (3, 4)	0.000000000000	0.000000000003	0.000000000000	−0.000000000012	0.000000000000
C_{33} (2, 5)	0.000000000007	0.000000000000	0.000000000001	0.000000000000	−0.000000000003
C_{36} (8, 0)	−0.000000000034	−0.000000000004	−0.000000000005	−0.000000000009	−0.000000000009
C_{38} (6, 2)	−0.000000000001	0.000000000000	0.000000000000	0.000000000000	0.000000000000
C_{44} (0, 8)	−0.000000000034	−0.000000000003	−0.000000000006	−0.000000000007	−0.000000000012

points. In contrast, the proposed machining program used a linear regression model to correct points by moving in both the x- and z-axis directions; as a result, the correction surfaces for approximately 10 million points were computed in 4 s, which is roughly ten times the number of points used in the conventional method. In multi-surface machining, the computation time increases proportionally with the number of optical surfaces. Nevertheless, the total time required to calculate the correction surfaces for all five optical surfaces was only 19 s, representing a 98.7% reduction in computation time compared with the conventional method.

The proposed machining program requires fitting of the XY polynomial to each corrected surface. Fig. 23 shows the fitting results for each correction surface. The fitting error directly affects the post-machining form error; however, the maximum PV and RMS values of the fitting error were 0.023 and 0.004 μm, respectively, confirming that the surface fitting was achieved with extremely high precision. The

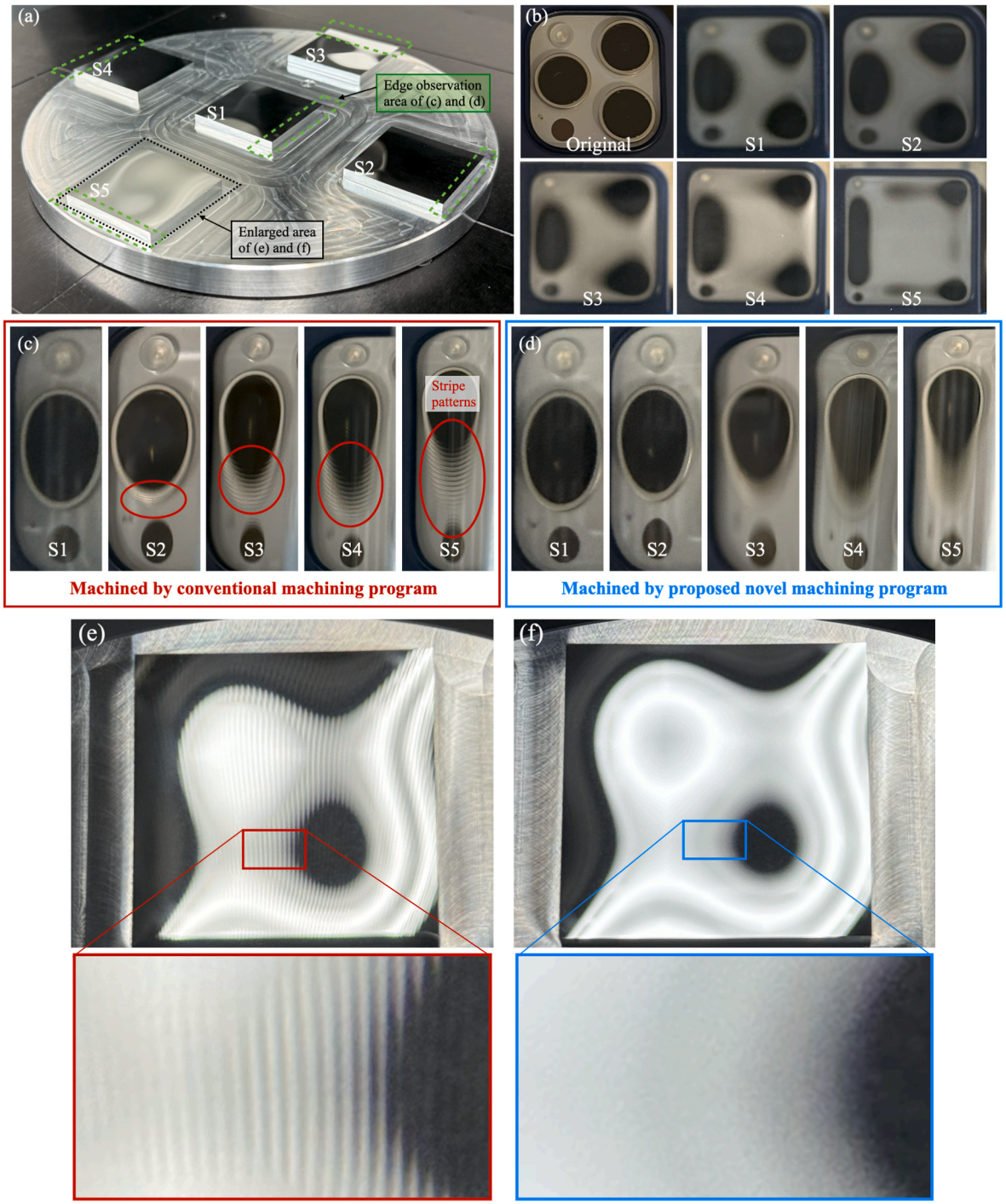

Fig. 24. (a) Overview of the machined surface and (b) reflected camera images of each freeform surface. Edge observation images of each freeform surface machined using the (c) conventional and (b) proposed machining programs. Comparison of S5 surface machined using the (e) conventional and (f) proposed machining programs.

resulting fitted coefficients of the XY polynomial for each correction surface are presented in Table 7. In the proposed machining program, the sum of the fitted coefficients (Table 7) and the original design coefficients (Table 6) is loaded as the corrected input for machining.

4.4. Surface topography results

The machine used in this experiment was the same as that in the basic cutting experiment (Section 3.3), and the specifications of the diamond tool and machining conditions were the same as those listed in Tables 3 and 4

Fig. 24 shows the machined surface images obtained by multi-surface machining. The optical surfaces are denoted as S1, S2, S3, S4, and S5. Fig. 24(a) shows an overall image of the machined sample, and Fig. 24(b) shows reflected camera images of each optical surface photographed from directly above. As shown in the designed surface in Fig. 19, higher-order optical surfaces were designed with larger height differences and greater curvature variations in the freeform geometry. The top-view images of the actual machined surfaces confirmed that the reflected camera image became significantly more distorted as the

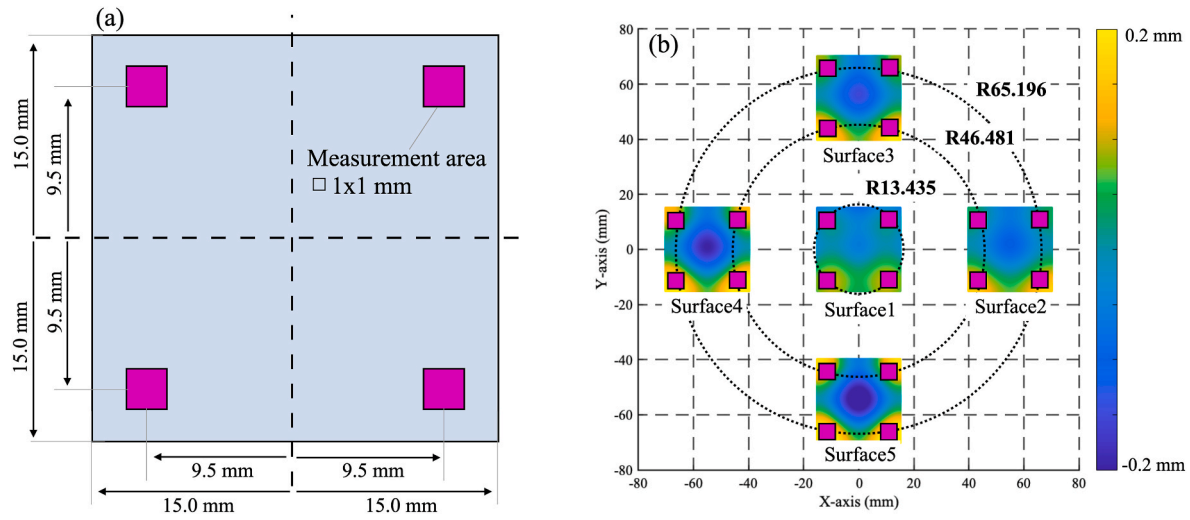

Fig. 25. Measurement areas and positions for (a) a single freeform surface and (b) the overall multi-surface layout.

curvature of the freeform surface increased, as shown in Fig. 24(b).

Additionally, Fig. 24(c) and (d) show images of the edges of each machined optical surface produced using the conventional bilinear interpolation method and the proposed direct-calculation machining program, respectively. The edge observation areas on each surface are indicated by green dotted lines in Fig. 24(a). As shown in Fig. 24(c), striped patterns appeared in the reflected camera images of the optical freeform surfaces machined using the conventional machining program. These stripe patterns, caused by interpolation errors in the point cloud surface definition, became increasingly distinct as the surface number increased and the curvature grew larger. In contrast, as shown in Fig. 24 (d), no such striped patterns appeared on the surfaces machined using the proposed machining program. This is because the actual design equation was evaluated during machining rather than approximating the design surface with a point cloud, resulting in a smooth surface free from stripe-pattern interpolation errors. A comparison of the S5 surfaces shown in Fig. 24(e) and (f) highlights the differences between the two programs. The surface in Fig. 24(e), machined using the conventional bilinear interpolation program, exhibits a pronounced overall stripe pattern. In contrast, the surface in Fig. 24(f), machined using the proposed program, exhibits a smooth mirror finish without any stripe patterns. Lenses exhibiting visible stripe patterns are unsuitable for practical use, and the comparison of machined surface images clearly demonstrates that the proposed machining program is highly effective in resolving this problem.

4.5. Form error evaluation

The profiles of each optical surface were measured using a white-light interferometer, and the form errors were evaluated by aligning the measured data to the ideal profile. The measurement locations on each optical surface are shown in Fig. 25. The analyzed form error maps are shown in Fig. 26, where Fig. 26(a) shows the results for Surface 1. The form error maps reveal no significant differences between the conventional and proposed machining programs. The maximum PV values were 0.159 and 0.150 μm, respectively, a difference of only 0.009 μm, and the RMS values for both were 0.010 μm, indicating that Surface 1 achieved comparable machining accuracy with both methods. Surface 1 was the only surface positioned at the center of the workpiece, unlike the other four surfaces. As shown in Fig. 6, the constant-angle point cloud placement method produces higher point density near the center. Therefore, high-precision machining with small interpolation errors can be achieved near the center using point cloud-based machining programs. Because both methods performed high-precision machining near the center, similar results were obtained for Surface 1.

Fig. 26(b), (c), 26(d), and 26(e) show the form error analysis results for Surfaces 2, 3, 4, and 5, respectively. Unlike Surface 1, the form errors of surfaces machined using the conventional bilinear interpolation program exhibited a linear pattern. This is attributed to interpolation errors, as these four surfaces were located at the outer periphery of the workpiece, where the point cloud density is lower than that of the central region. In contrast, the surfaces machined using the proposed machining program did not exhibit such characteristic error patterns. This is because the proposed method defines the surface directly from the design equation rather than from point cloud data, thereby avoiding the characteristic interpolation error patterns inherent in point cloud-based machining and enabling high-precision machining.

The PV and RMS form error values are summarized as bar graphs for each surface and distance from the workpiece center in Fig. 27, where Fig. 27(a) and (b) show the PV and RMS values for each surface, respectively. With the conventional bilinear interpolation method, the average PV and RMS values increased proportionally with the surface index, because surfaces with higher indices exhibit greater height variations and increased curvature. As illustrated in Fig. 28, regions of high curvature result in large elevation differences between adjacent points, thereby producing larger interpolation errors. In contrast, the proposed method exhibited minimal variation in the average PV and RMS values across all machined surfaces, demonstrating stable machining accuracy independent of surface curvature and clearly outperforming the conventional interpolation approach. For Surface 5, which exhibited the highest curvature, the proposed method reduced the average PV and RMS values by 32.8% and 58.7%, respectively, compared with the conventional bilinear interpolation method. Unlike the conventional method, in which machining accuracy degrades with increasing surface curvature, the proposed method was confirmed to be free from curvature dependency.

Fig. 27(c) and (d) show the PV and RMS form error values summarized as bar graphs with respect to the distance from the workpiece center. With the conventional method, the average PV and RMS values increased proportionally with the distance from the center, whereas the proposed method showed only minor variations. This trend in the conventional method arises because the point cloud density decreases with increasing distance from the workpiece center, resulting in deteriorating form accuracy toward the outer regions, as indicated in Fig. 27(c) and (d). In contrast, the machining accuracy of the proposed method did not exhibit such dependence on point cloud density, as the surface geometry was defined directly by the design equation rather than by discrete point clouds. At a distance of 65.196 mm from the center, the farthest of the

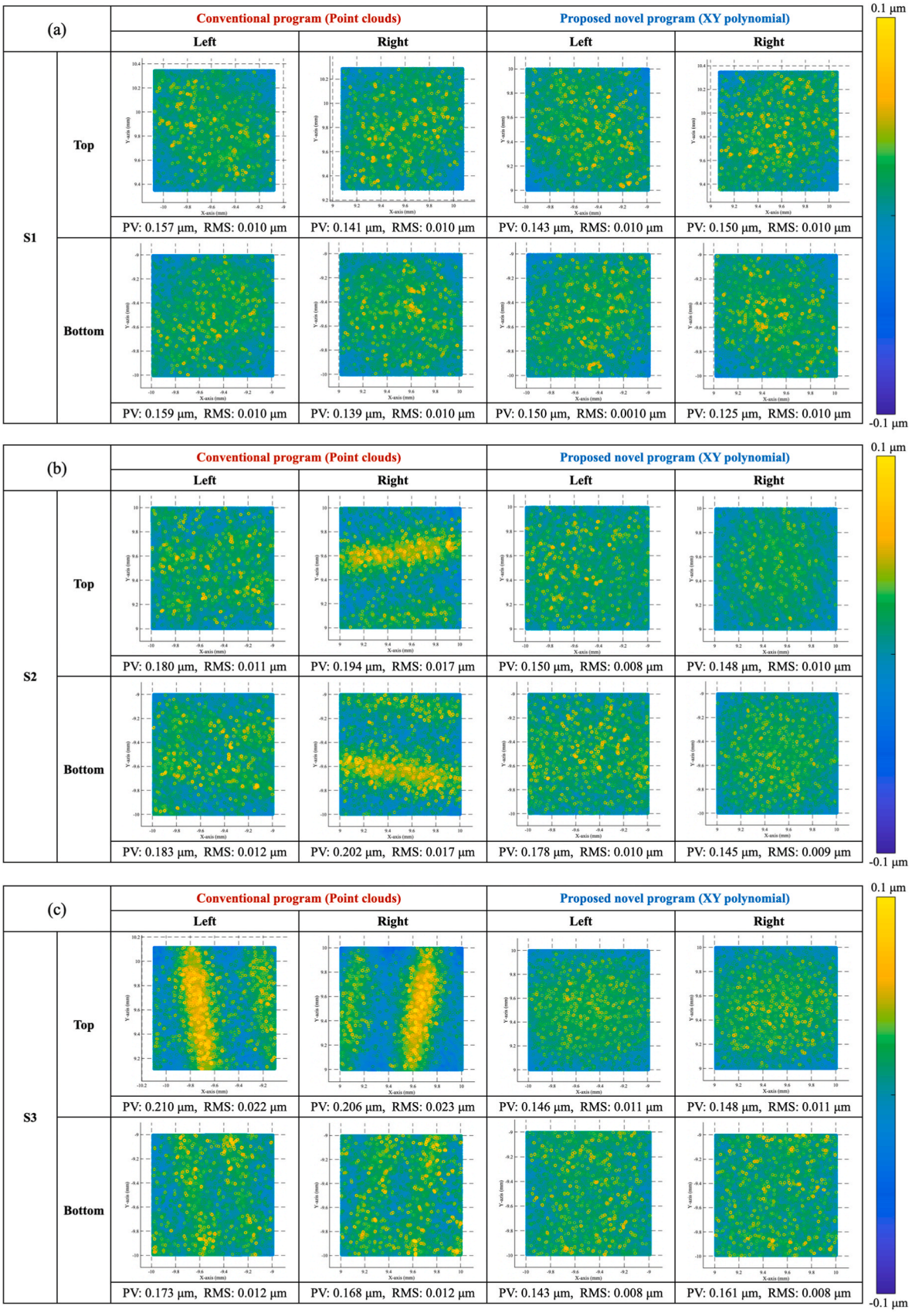

Fig. 26. Evaluated form error results of (a) S1, (b) S2, (c) S3, (d) S4, and (e) S5 surfaces machined using the conventional machining program with point cloud data and the proposed machining program with coefficient data.

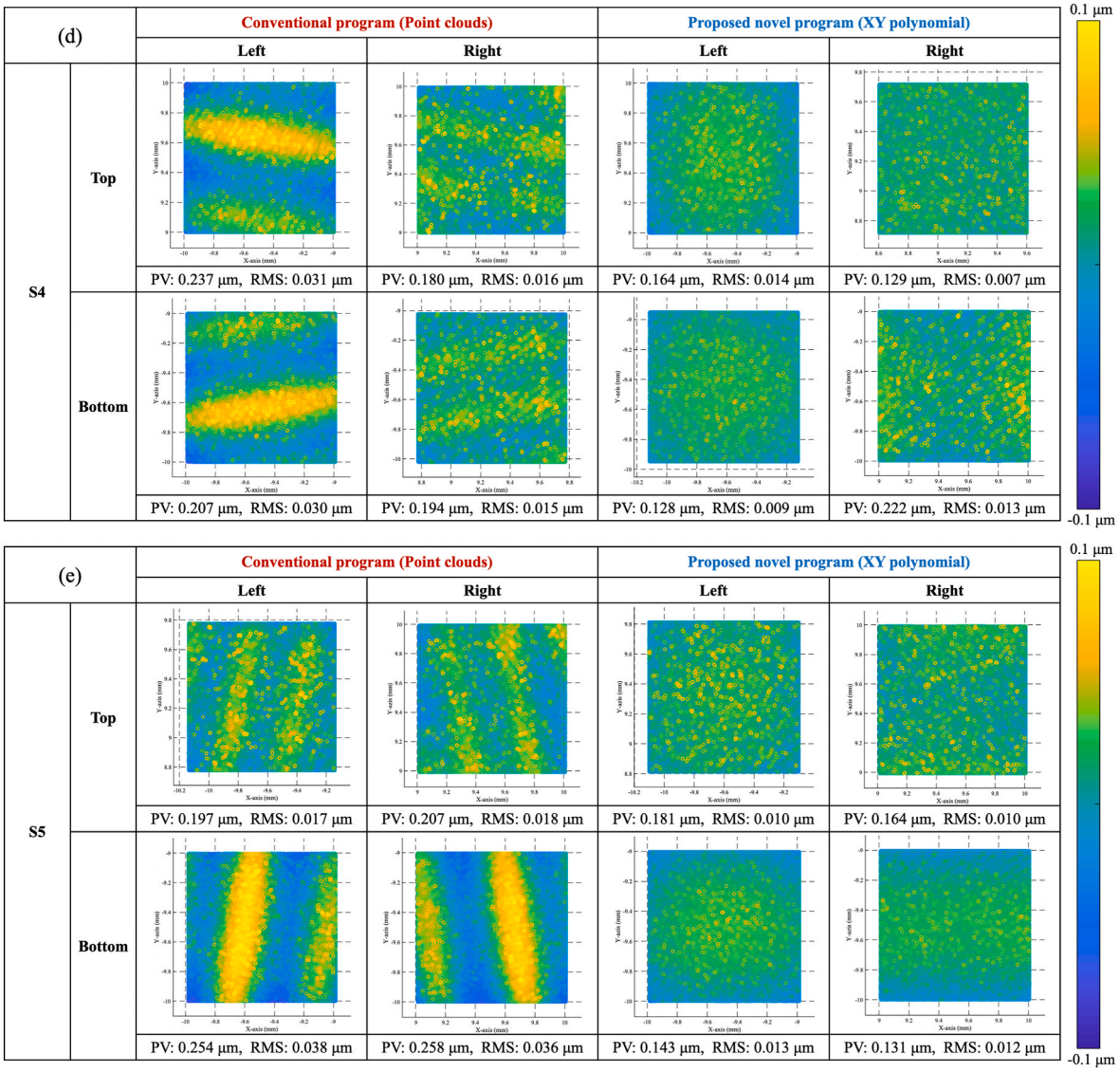

Fig. 26. (*continued*).

three evaluated distances, the proposed method reduced the average PV and RMS values by 34.8% and 58.4%, respectively, compared with the conventional bilinear interpolation method. These results demonstrate that the proposed method enables high-precision, stable machining irrespective of the machining location.

5. Conclusions

A novel machining program that directly evaluates the design equation during machining was proposed to suppress form errors caused by interpolation errors in conventional point cloud-based programs using bilinear interpolation. The effectiveness of the proposed method was verified through cutting experiments. The main conclusions of this study are summarized below.

(1) An XY polynomial equation was adopted to define the proposed machining program. This equation is widely used in the design of freeform optical surfaces and can express various complex freeform surfaces by adjusting the coefficients. It is also advantageous from the perspective of optical surface machining because surfaces can be easily combined, expanded, and scaled.

(2) A fast and accurate fitting method based on the XY polynomial equation was developed by applying a pseudoinverse matrix and coordinate normalization. By applying this method to the corrected point cloud data corresponding to the tool radius, the coefficients can be compensated from their original design values.

(3) Tool radius compensation was conducted for both the conventional and proposed machining programs. The calculation times for tool radius compensation using the conventional machining program were 1440 s and 1510 s for the single- and multi-surface experiments, respectively, whereas those for the proposed machining program were less than 5 s for a single freeform surface and 19 s for five freeform surfaces.

(4) Radial patterns were observed on the surfaces machined using the conventional machining program. In contrast, the surfaces machined using the proposed machining program did not exhibit such characteristic patterns and showed a smooth mirror finish.

(5) The form error evaluation results for single freeform surface machining clearly demonstrate the effectiveness of the proposed machining program. Compared with the conventional machining program, the proposed method reduced the PV and RMS form errors by 62.4% and 75.7%, respectively.

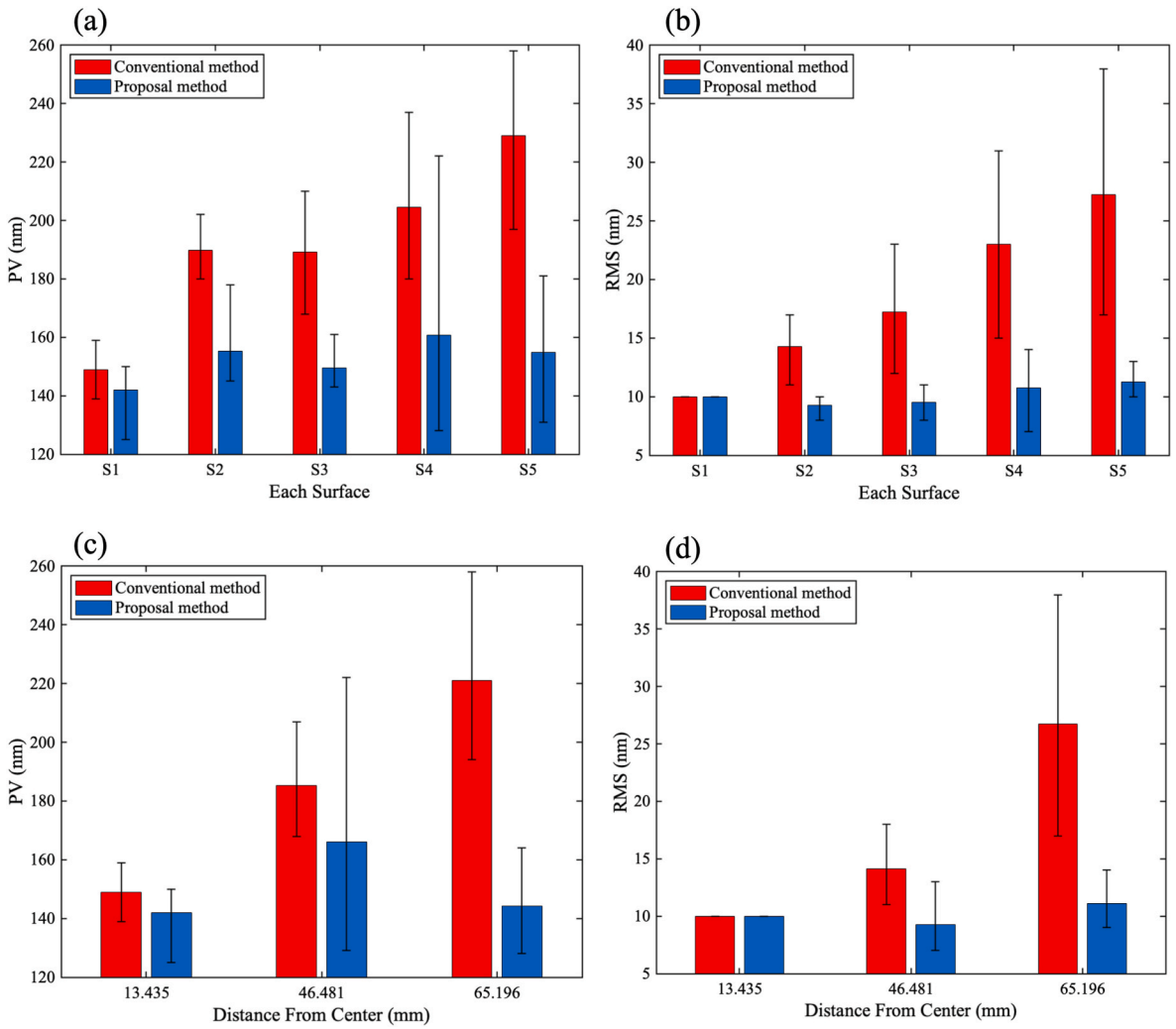

Fig. 27. Bar graphs of (a) PV and (b) RMS values of the evaluated form errors for each freeform surface, and (c) PV and (d) RMS values as a function of distance from the workpiece center.

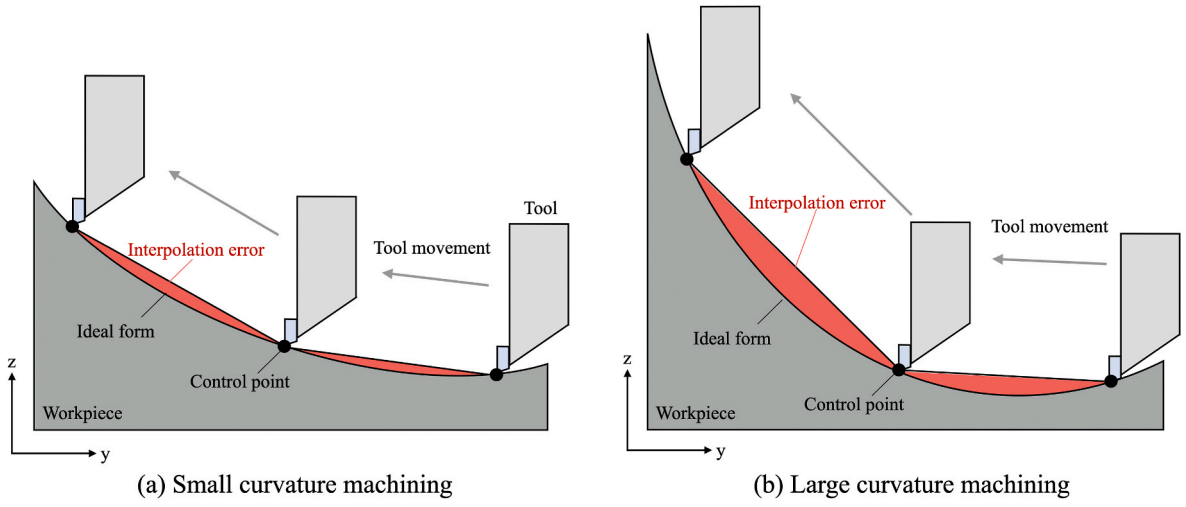

Fig. 28. Schematic illustrating the correlation between design surface curvature and interpolation error.

(6) A multi-surface machining experiment was conducted, and the proposed machining program was confirmed to achieve stable, high-precision machining regardless of the machining location or surface curvature.

The proposed machining program differs fundamentally from conventional point cloud-based approaches in that the optical design equation is directly evaluated during machining, eliminating the need for discrete point cloud representations. The proposed method achieved superior form accuracy by replacing a point cloud consisting of 993,600 points with only 20 coefficients. Because the proposed machining program is not subject to point cloud number limitations, its advantage becomes increasingly significant as the workpiece size increases. This approach offers an effective solution for manufacturing complex and large freeform surfaces with high form accuracy and efficiency. Further investigation, including validation against different interpolation strategies and optimized point cloud approaches, will be conducted in future work.

CRediT authorship contribution statement

Shigeru Tanikawa: Conceptualization, Data curation, Investigation, Methodology, Writing – original draft. **Jiwang Yan:** Resources, Supervision, Writing – review & editing.

Declaration of competing interest

The authors declare that they have no known competing financial interests or personal relationships that could have appeared to influence the work reported in this paper.

Acknowledgements

This work has been partially supported by Japan Society for the Promotion of Science under the Grant-in-Aid for Scientific Research (A), project number 25H00709.

References

[1] Pant LM, et al. Development of cubic freeform optical surface for wavefront coding application for extended depth of field infrared camera. Infrared Phys Technol 2022;127(Dec). https://doi.org/10.1016/j.infrared.2022.104377.
[2] Zhenrong Z, Xiang H, Xu L. Freeform surface lens for LED uniform illumination. Appl Opt 2009;48:6627–34. https://doi.org/10.1364/AO.48.006627.
[3] Fang FZ, Zhang XD, Weckenmann A, Zhang GX, Evans C. Manufacturing and measurement of freeform optics. CIRP Ann Manuf Technol 2013;62(2):823–46. https://doi.org/10.1016/j.cirp.2013.05.003.
[4] Forbes GW. Characterizing the shape of freeform optics. Opt Express 2012;20:2483–99. https://doi.org/10.1364/OE.20.002483.
[5] Sorgato S, et al. Custom freeform optics for LiDAR applications: from design to fabrication. Optical Design Eng IX 2024;13019. https://doi.org/10.1117/12.3017565. SPIE.
[6] Wei S, Zhu Z, Ma D. Efficient and compact freeform optics design for customized LED lighting. Opt Laser Technol 2023;167(Dec). https://doi.org/10.1016/j.optlastec.2023.109775.
[7] Chen B, Wei C, Shao J. Freeform optics in applications such as AR-HMD, automotive AR-HUD, and TMA telescope. Optical Design and Testing XIII 2023;12765. https://doi.org/10.1117/12.2689331. SPIE.
[8] Wang Y, Yang T, Lyu X, Cheng D, Wang Y. Ultra-simplified and low-cost head-up display system enabled by freeform holographic element. Opt Laser Technol 2024;178(Nov). https://doi.org/10.1016/j.optlastec.2024.111253.
[9] Jahn W, Ferrari M, Hugot E. Innovative focal plane design for large space telescope using freeform mirrors. Optica Oct. 2017;4(10):1188. https://doi.org/10.1364/optica.4.001188.
[10] You K, Liu G, Wang W, Fang F. Laser assisted diamond turning of silicon freeform surface. J Mater Process Technol 2023;322(Dec). https://doi.org/10.1016/j.jmatprotec.2023.118172.
[11] Mukaida M, Yan J. Ductile machining of single-crystal silicon for microlens arrays by ultraprecision diamond turning using a slow tool servo. Int J Mach Tool Manufact 2017;115(July 2016):2–14. https://doi.org/10.1016/j.ijmachtools.2016.11.004.
[12] Zuo C, et al. Diamond turning of freeform surfaces using non-zero rake angle tools. Int J Adv Manuf Technol 2022;118:2265–84. https://doi.org/10.1007/s00170-021-07890-x.
[13] Luo X, Liu Q, Madathil AP, Xie W. Predictive digital twin-driven dynamic error control for slow-tool-servo ultraprecision diamond turning. CIRP Ann Jan. 2024;73(1):377–80. https://doi.org/10.1016/j.cirp.2024.04.080.
[14] Nagayama K, Yan J. Deterministic error compensation for slow tool servo-driven diamond turning of freeform surface with nanometric form accuracy. J Manuf Process March 2020;64:45–57. https://doi.org/10.1016/j.jmapro.2021.01.015. 2021.
[15] Zhu Z, et al. Design and control of a piezoelectrically actuated fast tool servo for diamond turning of microstructured surfaces. IEEE Trans Ind Electron Aug. 2020;67(8):6688–97. https://doi.org/10.1109/TIE.2019.2937051.
[16] Huang WW, Zhang X, Zhu LM. Band-stop-filter-based repetitive control of fast tool servos for diamond turning of micro-structured functional surfaces. Precis Eng Sep. 2023;83:124–33. https://doi.org/10.1016/j.precisioneng.2023.05.008.
[17] Tanikawa S, Sato Y, Yan J. A novel calibration method for angular misalignment in independently controlled fast tool servo-based diamond turning. Precis Eng Sep. 2023;83:216–27. https://doi.org/10.1016/j.precisioneng.2023.06.010.
[18] Hashimoto T, Yan J. Time delay compensation in high-speed diamond turning of freeform surface using independent fast tool servo with a long stroke. Precis Eng May 2025;93:515–27. https://doi.org/10.1016/j.precisioneng.2025.02.006.
[19] Tian F, Yin Z, Li S. A novel long range fast tool servo for diamond turning. Int J Adv Manuf Technol 2016;86(5–8):1227–34. https://doi.org/10.1007/s00170-015-8282-9.
[20] Buhmann M, Carelli E, Egger C, Frick K. Point cloud based tool path generation for corrective machining in ultra-precision diamond turning. Int J Adv Manuf Technol 2022;120(9–10):6891–907. https://doi.org/10.1007/s00170-022-09033-2.
[21] Scheiding S, et al. Freeform manufacturing of a microoptical lens array on a steep curved substrate by use of a voice coil fast tool servo. Opt Express 2011;19(24):23938–51. https://doi.org/10.1364/OE.19.023938.
[22] Tanikawa S, Yan J. Fabrication of micro-structured surface with controllable randomness by using FTS-based diamond turning. Precis Eng Jan. 2022;73:363–76. https://doi.org/10.1016/j.precisioneng.2021.10.005.
[23] Peng Y, Ding H, Zhang D, Luo M. Calculation of tool offset and tool radius errors based on on-machine measurement and least squares method in ultra-precision diamond turning. Photonics Nov. 2024;11(11). https://doi.org/10.3390/photonics11111022.
[24] Chen C-C, Huang C-Y, Peng W-J, Cheng Y-C, Yu Z-R, Hsu W-Y. Freeform surface machining error compensation method for ultra-precision slow tool servo diamond turning. Optical manufacturing and testing X, 8838; 2013. p. 88380Y. https://doi.org/10.1117/12.2022981.
[25] Wang D, Sui Y, Yang H, Li D. Adaptive spiral tool path generation for diamond turning of large aperture freeform optics. Materials 2019;12(5). https://doi.org/10.3390/MA12050810.
[26] Guo Y, et al. Spiral tool path optimization method for fast/slow tool servo-assisted diamond turning of freeform surfaces with highly form accuracy. Precis Eng Mar. 2023;80:229–42. https://doi.org/10.1016/j.precisioneng.2022.12.007.
[27] Zhang L, Sato Y, Yan J. Optimization of fast tool servo diamond turning for enhancing geometrical accuracy and surface quality of freeform optics. J Adv Mech Des Syst Manuf 2023;17(1). https://doi.org/10.1299/jamdsm.2023jamdsm0012.
[28] Oka K, Sparrold S. Asphere design for dummies. Novel Optical Systems Design and Optimization XV 2012;8487:84870B. https://doi.org/10.1117/12.930989.
[29] Kweon G-I, Kim C-H. Aspherical Lens design by using a numerical analysis. J Kor Phys Soc 2007;51(1):93–103. https://doi.org/10.3938/jkps.51.93.
[30] Zhou T, et al. Machine learning for aspherical lens form accuracy improvement in precision molding of infrared chalcogenide glass. Precis Eng Oct. 2024;90:156–63. https://doi.org/10.1016/j.precisioneng.2024.08.007.
[31] Traub M, Hoffmann D, Hengesbach S, Loosen P. Automatic design of multi-lens optical systems based on stock lenses for high power lasers. International Optical Design Conference 2014 2014;9293:92931I. https://doi.org/10.1117/12.2074508.
[32] Fan C, Yang B, Liu Y, Gu P, Wang X, Zong H. Zoom lens with high zoom ratio design based on Gaussian bracket and particle swarm optimization. Appl Opt Apr. 2021;60(11):3217. https://doi.org/10.1364/ao.418970.
[33] Zhang Z, et al. Precision glass molding technology for XY polynomial freeform optical elements with simulations and experiments. Opt Express Jun. 2024;32(13):22905. https://doi.org/10.1364/oe.525414.
[34] Li Z, Guan C, Dai Y, Yong J. Optical surface error analysis and compensation technique based on zernike polynomial coefficients. 10th international symposium on advanced optical manufacturing and testing technologies: advanced optical manufacturing and metrology technologies, 12071. SPIE; 2021. https://doi.org/10.1117/12.2604688.
[35] Schwiegerling J. Review of zernike polynomials and their use in describing the impact of misalignment in optical systems. Optical System Alignment, Tolerancing, and Verification XI 2017;10377. https://doi.org/10.1117/12.2275378. SPIE.
[36] Zhang Y, You K, Fang F. Pre-compensation of mold in precision glass molding based on mathematical analysis. Micromachines Dec. 2020;11(12):1–13. https://doi.org/10.3390/mi11121069.

[37] Lee D, et al. Thermal deformation compensation in the molding of aspheric glass lenses. Opt Eng Jun. 2014;53(6):065106. https://doi.org/10.1117/1.oe.53.6.065106.
[38] Lee WB, Cheung CF, Chiu WM, Leung TP. Investigation of residual form error compensation in the ultra-precision machining of aspheric surfaces. J Mater Process Technol 2000;99(1):129–34. https://doi.org/10.1016/S0924-0136(99)00403-3.
[39] Yu DP, Gan SW, Wong YS, Hong GS, Rahman M, Yao J. Optimized tool path generation for fast tool servo diamond turning of micro-structured surfaces. Int J Adv Manuf Technol 2012;63(9–12):1137–52. https://doi.org/10.1007/s00170-012-3964-z.
[40] Liu C, Xue C, Zhang Q, Liu X, Zhou P. Optimization method of tool path generation considering the edge of lenslets for a microlens array in FTS diamond turning. Appl Opt 2019;58(24):6713. https://doi.org/10.1364/ao.58.006713.
[41] Khatri N, Berwal S, Manjunath K, Singh B. Optical design and fabrication of zinc selenide microlens array with extended depth of focus for biomedical imaging. Nanofabrication 2023;8. https://doi.org/10.37819/nanofab.008.293.
[42] Sato Y, Yan J. Tool path generation and optimization for freeform surface diamond turning based on an independently controlled fast tool servo. Int J Extrem Manuf Jun. 2022;4(2). https://doi.org/10.1088/2631-7990/ac5f12.
[43] Hashimoto T, Yan J. Effect of system dynamics on surface topography in fast tool servo-based diamond turning of microlens arrays. Nanomanufacturing Metrol Dec. 2025;8(1). https://doi.org/10.1007/s41871-025-00253-0.